Henrique Akira Tajiri

Manufacturing and characterization of porous ceramic capillary membranes for enzyme functionalization through click chemistry

Dissertação submetido ao Programa de Pós-Graduação em Engenharia Química da Universidade Federal de Santa Catarina para a obtenção do Grau de Mestre em Engenharia Química.

Orientador:
Prof. Dr. Dachamir Hotza

Coorientadora:
M.Sc. Marieke Hoog Antink

Florianópolis
2018

Ficha de identificação da obra elaborada pelo autor,
através do Programa de Geração Automática da Biblioteca Universitária da UFSC.

Tajiri, Henrique Akira
Manufacturing and characterization of porous ceramic capillary membranes for enzyme functionalization through click chemistry / Henrique Akira Tajiri ; orientador, Dachamir Hotza, coorientador, Marieke Hoog Antink, 2018.
98 p.

Dissertação (mestrado) - Universidade Federal de Santa Catarina, Centro Tecnológico, Programa de Pós Graduação em Engenharia Química, Florianópolis, 2018.

Inclui referências.

1. Engenharia Química. 2. Capilares cerâmicos porosos. . 3. Funcionalização de superfície.. 4. Click chemistry.. 5. Atividade enzimática.. I. Hotza, Dachamir . II. Antink, Marieke Hoog . III. Universidade Federal de Santa Catarina. Programa de Pós-Graduação em Engenharia Química. IV. Título.

Henrique Akira Tajiri

Manufacturing and characterization of porous ceramic capillary membranes for enzyme functionalization through click chemistry

Esta Dissertação foi julgada adequada para obtenção do Título de "Mestre em Engenharia Química" e aprovada em sua forma final pelo Programa de Pós-Graduação em Engenharia Química da Universidade Federal de Santa Catarina.

Florianópolis, 22 de março de 2018.

_____
Prof. Cíntia Soares, Dr.ª
Coordenadora do Programa

Banca Examinadora:

_____
Alexsandra Valério, Dr.ª
POSENQ/UFSC

_____
Prof. Hazim Ali Al-Qureshi, Dr.
PGMAT/UFSC

Este trabalho é dedicado a Deus e à minha família que eu amo muito.

ACKNOWLEDGEMENTS

At first, I would like to thank God (the Father, the Son and the Holy Spirit) for His unfailing love, grace and mercy.

I thank the National Council for Scientific and Technological Development (CNPq) for the scholarship and for investing in the future of the Brazilian education and society.

I also thank Prof. Dr. Dachamir Hotza for being my supervisor and for always supporting me throughout my master program.

I thank Prof. Dr. rer. Nat. Kurosch Rezwan, for another opportunity to be part of the Advanced Ceramics group for 6 months.

I thank M. Sc. Marieke Hoog Antink for the research project she has proposed; for all the time she spent with me and all explanations she gave about the project, always being willing to help me and discuss important issues; and for all the support necessary to conduct the research.

I thank all the administrative staff, senior scientist, postdocs, PhD students, technical staff (Jürgen Horvath, Tina Kühn, Cristian Nuortila, and Gabriela Berger) and colleagues from the Advanced Ceramics group and the Graduate Program in Chemical Engineering from the Federal University of Santa Catarina for helping me and for the great time we spent together.

I thank Prof. Dr. Cíntia Soares and Edevilson Silva for their great zeal and commitment with the Graduate Program in Chemical Engineering from the Federal University of Santa Catarina.

Finally, I thank my family and brethren for always supporting my decisions, for helping me every time I needed them, and for their love and friendship.

“If I have the gift of prophecy and can fathom all mysteries and all knowledge, and if I have a faith that can move mountains, but do not have love, I am nothing.”
(Apostle Paul to the church of God in Corinth)

RESUMO

Capilares porosos feitos de zircônia foram fabricados e caracterizados combinando a técnica de moldagem por extrusão e material de sacrifício. Pastas cerâmicas, coloidalmente estáveis, de zircônia estabilizada com ítria com dois tamanhos de partículas, decano, hexano, ácido esteárico e cera de abelhas foram preparadas e extrudadas, gerando diferentes porosidades. Para conferir estabilidade mecânica, as amostras foram conduzidas a um tratamento térmico a 1438 K. A superfície dos microtubos cerâmicos foi funcionalizada para promover a *click chemistry* e imobilizar as enzimas funcionalizadas com grupos acetila. Além disso, a ativação hidrotérmica na superfície do cerâmico levou a um efeito benéfico para posterior deposição de APTES. A porosidade aberta das amostras variou de 50% a 56% e a permeação de fluxo de água de 140 até 388 L/(m^2.h.bar). Uma tensão de flexão de até 76 MPa foi medida para amostras feitas da mistura de pós de zircônia. Uma tendência pode ser observada: ao se diminuir o tamanho das partículas de zircônia, obteve-se uma melhora nas propriedades mecânicas dos corpos sinterizados. Por outro lado, a permeabilidade intrínseca diminuiu. A respeito da atividade enzimática, capilares feitos com tamanho de partículas maiores levaram a resultados melhores. Capilares porosos de zircônia apresentam um futuro promissor para aplicações onde enzimas imobilizadas em regime de fluxo são empregadas.

Palavras-chave: Capilares cerâmicos porosos. Funcionalização de superfície. *Click chemistry*. Atividade enzimática.

RESUMO EXPANDIDO

Introdução

Nutrientes são substâncias químicas não são sintetizadas pelo corpo humano provenientes dos alimentos. São importantes para a produção de energia e para manter as reações químicas que ocorrem para as funções básicas de sobrevivência tais como respiração, batimento cardíaco, locomoção, atividade cerebral, reprodução, entre outros. Proteínas são nutrientes formados por moléculas grandes e complexas, consistindo de cadeias de subunidades conhecidas como aminoácidos. Além de prover energia, proteínas também dão estrutura, transporte e conduzem a maioria das reações químicas que ocorrem no corpo humano. No tocante ao estado das proteínas, elas podem ser encontradas intactas ou hidrolisadas. Na ingestão, proteínas hidrolisadas aceleram o processo de digestão e absorção. Na indústria de alimentos, é comum que o processo de hidrólise das proteínas seja feito em processos de batelada e frequentemente em processos de fermentação e ou onde enzimas são utilizadas. Produção de cerveja, amaciamento de carne e produção de queijos são exemplos de processos onde ocorre a hidrólise de proteína em regime de batelada. Em processos de batelada, grandes reatores são geralmente usados, onde enzimas e substratos são adicionados e misturados sob temperatura constante, pH controlado e agitação contínua por diversas horas. A atividade enzimática é controlada pela alteração da temperatura e/ou do pH. É difícil, para regimes de batelada, manter um rigoroso controle do processo. Então, algumas propriedades do produto podem variar significativamente além do grande desperdício de enzimas que possuem um alto preço. Com o intuito de maximizar a eficiência econômica reduzindo gastos energéticos e financeiros usando enzimas de elevado preço, enzimas estabilizadas são pré-requisitos para um regime contínuo de produção. As enzimas podem ser estabilizadas via imobilização, engenharia de proteína, mudança química ou adicionando aditivos. Entre esses métodos, o mecanismo mais comum é a imobilização de enzima. Há muitas maneiras que as enzimas podem ser imobilizadas, porém a imobilização utilizando ligações covalentes apresenta um futuro promissor no uso industrial, pois a enzima está fortemente ligada ao suporte evitando perdas durante o processamento. Suportes cerâmicos porosos são reportados na literatura apresentando propriedades tais como grande proporção de área superficial em relação ao volume, altas taxas de transferência de massa e de acessibilidade às enzimas. Geralmente, membranas poliméricas são mais usadas na indústria devido ao seu baixo custo; no entanto, membranas cerâmicas apresentam porosidade controlada, boa resistência mecânica, resistência química, e estabilidade

sob altas temperaturas e pressão, tornando-se suportes atraentes para aplicações usando enzimas imobilizadas.

Objetivos

Este trabalho tem como objetivos a produção e a caracterização de capilares cerâmicos com diferentes porosidades, variando o tamanho inicial das partículas e combinando a técnica de material de sacrifício e moldagem por extrusão; a funcionalização e a caracterização dos microtubos cerâmicos; a funcionalização das enzimas; a imobilização das enzimas na superfície dos capilares utilizando a técnica *click chemistry*; a avaliação da atividade enzimática em regimes de batelada e fluxo contínuo; a determinação da composição ótima para a melhor performance das enzimas.

Metodologia

Para a produção de capilares cerâmicos porosos, pós de zircônia estabilizada por ítria de diferentes tamanhos, cera de abelha, ácido esteárico, decano e hexano foram usados como matérias primas para a extrusão dos microtubos. Após extrudados e sinterizados, esses capilares cerâmicos foram funcionalizados para que grupos azidas estivessem ligados à sua superfície para posterior *click chemistry* com as enzimas previamente modificadas. Os pós cerâmicos foram caracterizados utilizando microscopia eletrônica de varredura, espalhamento dinâmico de luz, picnometria a hélio, e BET. Já os capilares cerâmicos foram caracterizados usando microscopia ótica e eletrônica de varredura, determinação de densidade e de porosidade aberta, porosimetria por intrusão de mercúrio, BET, ensaio de flexão de três pontos, teste de permeação de fluxo de água, quantificação de grupos amino e determinação de atividade enzimática sob condições de batelada e de fluxo contínuo.

Resultados e Discussão

Os pós de zircônia se apresentaram de forma aglomerada, devido ao seu reduzido tamanho de partícula e consequentemente, elevada área superficial, ou seja, reatividade. Com relação a densidade e área superficial desses pós, os valores medidos estão de acordo com os dados do fabricante e dos dados encontrados na literatura. Os capilares cerâmicos apresentaram uma densificação parcial, onde dois grupos de tamanho de poros distintos puderam ser notados: um referente ao espaço entre as partículas de zircônia e outro referente ao material de sacrifício. Notou-se que o aumento do tamanho de pó inicial levou a uma diminuição

da retração, da densificação e da tensão de flexão, porém observou-se um aumento na percentagem de poros abertos e na permeação do fluxo de água. Não foi possível observar a Lei das Misturas para as propriedades das amostras feitas usando a mistura de pós. Ainda referente à mistura de pós cerâmicos, essa composição gerou amostras que exibiram a maior densidade e tensão de flexão. Supõe-se que, devido a mistura dos pós, houve um melhor empacotamento das partículas favorecendo o processo de sinterização e explicando-se assim esses resultados. A porosidade aberta e o tamanho de pós apresentaram uma influência importante nas propriedades de permeação de fluxo de água; já a densidade e porosidade aberta ajudaram a determinar o comportamento mecânico das amostras. Em relação à deposição de grupos amino na superfície dos capilares não foi possível notar uma diferença significante ao se alterar a composição química, consequentemente, a porosidade aberta. E referente à atividade enzimática, no regime de batelada, notou-se que as amostras submetidas a todo o processo de funcionalização (deposição de APTES e deposição de grupos azida) e *click chemistry* apresentaram um comportamento mais estável quando comparadas às amostras somente hidroxiladas, sugerindo assim o cumprimento do papel da *click chemistry* (formação de ligações covalentes) na imobilização da enzima. No regime de fluxo, as amostras praticamente não apresentaram atividade enzimática, com exceção das amostras feitas com o maior tamanho de partícula de zircônia e modificadas com o *click chemistry*. Algumas hipóteses puderam ser estabelecidas consoante a estes resultados: altas pressões foram alcançadas enquanto a solução foi bombeada no microtubo, lixiviando as enzimas acopladas ao suporte cerâmico; essa total lixiviação não foi notada para as amostras feitas com zircônia de maior tamanho de partícula e com *click chemistry* pois para esse tamanho de partícula, e para um determinado fluxo, essa condição apresentou menor pressão. Além disso, devido à forte ligação covalente proveniente do *click chemistry*, as enzimas puderam resistir à pressão do fluido durante o regime contínuo de teste.

Considerações Finais

Microtubos porosos feitos de zircônia estabilizada por ítria foram produzidos com sucesso combinando a moldagem por extrusão e a técnica de técnica de material de sacrifício. A pasta cerâmica produzida apresentou um comportamento de estabilidade coloidal em meio básico. Em relação à produção dos capilares, notou-se que o aumento do tamanho inicial do pó levou a um aumento da percentagem de poros abertos, da densidade e da permeação de fluxo de água; entretanto, levou a uma

deterioração das propriedades mecânicas. A mistura dos pós de zircônia produziu capilares com as maiores densidade e tensão de flexão. No tocante à imobilização das enzimas no suporte, não foi possível notar uma diferença significante do número de grupos amino acessíveis, variando a composição da amostra. Os resultados de atividade enzimática mostraram que a atividade enzimática é favorecida para amostras com tamanho de poros e percentagem de porosidade mais elevada e amostras com *click chemistry* apresentaram um comportamento mais estável. A composição ótima para as amostras foi zircônia com maior tamanho de partícula e usando a técnica de imobilização *click chemistry*. Como trabalhos futuros, sugere-se produzir capilares utilizando outros materiais de sacrifício, variando assim a porosidade, usar outras técnicas de caracterização para os tubos funcionalizados e conduzir experimentos de atividade enzimática usando outros parâmetros.

Palavras-chave: Capilares cerâmicos porosos. Funcionalização de superfície. *Click chemistry*. Atividade enzimática.

ABSTRACT

Porous zirconia capillaries were fabricated and characterized combining extrusion molding and sacrificial template technique. Colloidally stable ceramic pastes made of two yttria-stabilized zirconia particle sizes, decane, hexane, stearic acid and beeswax were prepared and extruded, leading to different porosities. To confer mechanical stability to the monoliths, a thermal treatment was conducted at 1438 K. The surface of the ceramic microtubes was functionalized in order to promote click chemistry and immobilize acetylene functionalized enzymes on it. Furthermore, introducing a hydrothermal activation on the ceramic surface had a beneficial effect on further deposition of APTES. The open porosity of the samples ranged from 50 to 56% and water permeate flux from 140 up to 388 L/(m^2.h.bar). Characteristic flexural strength up to 76 MPa was recorded for the samples with the blend of the zirconia powders. Moreover, a trend could be observed, decreasing the zirconia particle size enhanced the mechanical strength of the sintered bodies. On the other hand, the intrinsic permeability has decreased. Regarding to enzyme activity, capillaries with larger zirconia particle size led to better enzyme activity results. Porous zirconia capillaries show a promising future for immobilized enzyme applications under flow regime.

Keywords: Porous ceramic capillaries. Surface functionalization. Click chemistry. Enzyme activity.

LIST OF FIGURES

LIST OF CHARTS

LIST OF TABLES

LIST OF ABBREVIATIONS

APTES – (3 aminopropyl)triethoxysilane
BSA – Bovine Serum Albumin
BET – Brunauer, Emmett and Teller
CAS – Chemical Abstracts Number
CuAAC – Copper-catalyzed azide-alkyne cycloaddition
DH – Capillary hydrothermally activated
DHFE – Capillary hydrothermally activated and functionalized in ethanol
DHFT – Capillary hydrothermally activated and functionalized in toluene
DHFW – Capillary hydrothermally activated and functionalized in water
DLS – Dynamic Light Scattering
DMF – Dimethylformamide
DR – Capillary without hydroxylation
DRFE – Capillary without hydroxylation and functionalized in ethanol
DRFT – Capillary without hydroxylation and functionalized in toluene
DRFW – Capillary without hydroxylation and functionalized in water
EDC – (3-dimethylaminopropyl)-N-ethylcarbodiimide
IEP – Isoelectric point
IUPAC – International Union of Pure and Applied Chemistry
MES – 2-(N-Morpholino)ethanesulfonic
NHS – Hydroxysuccinme
SEM – Scanning Electronic Microscopy
TCA – Trichloroacetic acid solution
YSZ – Yttria-stabilized zirconia

LIST OF SYMBOLS

α – Contact angle
ρ_{bulk} – Bulk density
ρ_s – Apparent density
γ – Surface tension
μ - Absolute viscosity
σ_f – Flexural strength
σ_{3PB} – Characteristic flexural strength
θ – Open porosity
$\theta_{theoretical}$ – Theoretical density

SUMMARY

1 INTRODUCTION

In human health, nutrients are chemical substances that are not synthesized by the human body, but they come from the food. Furthermore, nutrients are pivotal to produce energy to keep the chemical reactions taking place for the basic living functions such as breathing, moving, reproducing, heart beating, brain working, and others (Zimmerman e Snow, 2012).

There are six classes of essential nutrients needed daily to maintain and develop a healthy body: carbohydrates, lipids, proteins, water, vitamins, and minerals. Moreover, within these classes they can be divided into two groups: micro and macronutrients. Micronutrients are chemical substances needed in few amounts, which are employed to assist in the process as being part of enzymes. Micronutrients consist of vitamins and minerals. On the other hand, macronutrients are nutrients required in larger quantities and they act as source of energy to the body. Macronutrients include carbohydrates, lipids, and proteins (Medicine, 2005; Zimmerman e Snow, 2012).

Proteins are complex and large molecules (macromolecules) consisting of chains of subunits called amino acids. Besides providing energy, proteins also grant structure, transport, and conduct most of the chemical reaction which occurs in the body (Turnbough e Martos, 2003; Zimmerman e Snow, 2012). Regarding to the state of the protein, two types of proteins are found: hydrolysate and intact protein. In addition, for ingestion, the former has been expected to speed protein digestion and absorption (Koopman *et al.*, 2009).

In food industry, it is common that protein hydrolysis is done in batch processes and frequently used in fermentation and enzyme-based process (Sewczyk *et al.*, 2018). Brewing, meat tenderization, baking and cheese manufacturing are examples of protein hydrolysis carried out in batch regime (Godfrey e Reichelt, 1982). In batch process, usually, large reactors are used where enzymes and substrates are poured in and mixed under constant temperature, controlled pH, and continuous stirring for several h. The enzyme activity is controlled by changing the temperature and/or shifting the pH. It is difficult for these batch regimes to keep a meticulous control throughout the entire process; therefore it is noticeable a variation of product properties and huge amounts of high-priced enzymes used only one time (Pasupuleti e Braun, 2010; Hou *et al.*, 2017; Sewczyk *et al.*, 2018).

In pursuance of maximizing economic efficiency by reducing energy expenditure and enzyme costs, stabilized enzymes are required

under a continuous production regime. There are several ways in which the enzymes can be stabilized. For instance, it can be done by immobilization, protein engineering, chemical modification, protein engineering or adding additives. Among the cited methods, the most common mechanism is enzyme immobilization on a solid support (Moehlenbrock e Minteer, 2017; Sewczyk *et al.*, 2018). In the literature, four categories of enzyme immobilization techniques are frequently used: physical adsorption, entrapment, covalent bonding, and cross-linking (Hanefeld *et al.*, 2009; Datta *et al.*, 2013; Mohamad *et al.*, 2015).

Covalent biding of an enzyme to a solid support shows a promising future in the enzyme industry, because the enzyme is fast linked to the support minimizing the enzyme leaching during the process (Hanefeld *et al.*, 2009). Even though the enzyme loss is avoided with the covalent biding, the activity of the enzyme can decrease after immobilization, being a dilemma for enzyme catalysis (Ai *et al.*, 2014).

Researches acknowledge that it is also crucial to choose the best solid support (Zheng *et al.*, 2015). For instance, highly porous support, such as ceramic capillary, is claimed to be a good support for enzyme applications since it provides a large surface area in proportion to its volume, yielding a higher mass transfer and enzyme accessibility (Datta *et al.*, 2013; Sewczyk *et al.*, 2018). Generally, polymeric membranes are more frequent in industry due to its inexpensiveness; nevertheless, ceramic membranes present the possibility to tailor its porosity (i.e. narrow pore size distribution and higher porosity), good mechanical strength, chemical resistance and stability under high pressures and temperatures (Lee *et al.*, 2015). Within the ceramic materials, yttria-stabilized zirconia shows to be promising as the ceramic support, since it features high fracture toughness and strength when compared to other ceramic oxide materials (e.g. alumina) (Reed, 1995).

Some approaches are used to activate the ceramic membranes. First, due to the low quantity of hydroxyl groups on the surface of zirconia microtubes, they can be hydroxylated via autoclave, acidic, and alkaline hydroxylation (Kroll *et al.*, 2012). Once the hydroxyl concentration is increased, the ceramic membranes are ready to be chemically modified. Silanization with 3-aminopropyltriethoxysilane is one way to chemically modify the surface of the ceramic (Kroll *et al.*, 2010).

The activated enzyme should be linked to the functionalized ceramic porous capillary. One way, reported in the literature recently, to covalently bind an enzyme to a ceramic support is using the click chemistry (Moses e Moorhouse, 2007). Thus, this is a novel work that aims to produce porous ceramic capillary with proteolytic enzyme

immobilized on its surface using click chemistry and evaluate the structural properties, enzyme activity and success of the chemical functionalization procedures under batch and continuous regimes.

2 THEORETICAL BACKGROUND

This section seeks to give the reader a broad theoretical framework for understanding the key points of the work. The unity is divided into five main sections, where the first section provides a concise overview about cellular ceramics; the second section deals with extrusion of ceramics body; the third gives a brief introduction about surface functionalization and click chemistry; the fourth one regards to enzymes; and the last one gives an overview of some characterization techniques used in this present work.

2.1 CELLULAR CERAMICS

The porosity in materials can be tailored in such way that it is possible to produce ceramics with well-defined and homogenous porosity. The three-dimensional arrangement of a substantial quantity of pores featuring specific shape leads to a solid monolith presenting the so-called cellular structure (Scheffler e Colombo, 2005). The word 'cell' comes from the Latin *cella*, meaning a small compartment, cavity, or bounded space. Therefore a group of cells can lead to cellular solid (Gibson e Ashby, 1988; Merriam-Webster, 2018).

For a long time, porosity has been claimed to be an issue in technical ceramics; nevertheless, the latent benefits offered by porous ceramics are attracting more attention (Julbe *et al.*, 2001; Scheffler e Colombo, 2005; Deville, 2008). These promising advantages emerged once cellular ceramics can be engineered into specific architectures possessing intrinsic benefits such as increased surface area, better control of heat within the structure, permeability, and maximization of the strength/density ratio (Scheffler e Colombo, 2005). For instance, many materials found and analyzed in nature present a cellular structure and consequently have a considerable amount of porosity, which is essential for optimizing their properties for a particular function (Gibson e Ashby, 1988; Scheffler e Colombo, 2005).

It is possible to produce pores with different shape, size, and interconnectivity. With respect to the shape of the pores, they can be classified as: cylindrical, open or blind, ink-bottle shaped, funnel shaped, and slit-shaped. Regarding the size of the porosity, porous material can be referred as: microporous materials when pore diameters are less than 2 nm; mesoporous materials for pore diameters between 2 and 50 nm; and macroporous materials, in which pore diameters are greater than 50 nm. In respect of the interconnectivity of the pores they can be classified as

closed or opened pores (which can be in turn blind pores or through pores) (Rouquerol *et al.*, 1994). The different shapes and interconnectivities of the pores are illustrated in the Figure 1.

Figure 1: Schematic cross-section of a porous solid. The red contents refer to the interconnectivity of the pores while the green contents refer to the shape of the pores.

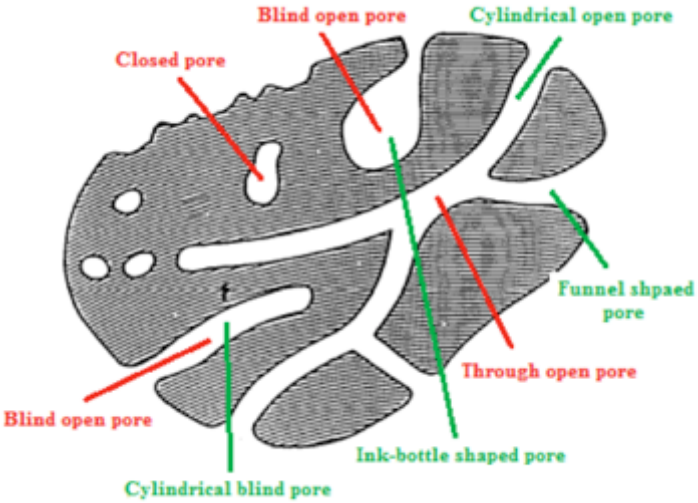

Source: Adapted from (Rouquerol *et al.*, 1994).

With respect to pore size, microporous and mesoporous materials present a potential application in ion exchange, separation and catalysis, insulation, drug delivery, and also as sensors, lasers, low conductivity substrates for electronics application, and as electrode materials (Akhtar *et al.*, 2014). On the other hand, macroporous materials are used for thermal insulation, packing, buoyancy, filtration, and structural applications (Gibson e Ashby, 1988; Akhtar *et al.*, 2014).

There are many different methods to produce porous ceramics. Therefore, it is important to bear in mind that every processing route is intrinsically limited to a narrow range of porous characteristics. The typical processing methods include: replica technique, direct foaming, and sacrificial template method, as illustrated in Figure 2 (Studart *et al.*, 2006).

Figure 2: Examples of typical processing routes to produce macroporous materials, including replica (a), sacrificial template (b), and direct foaming (c).

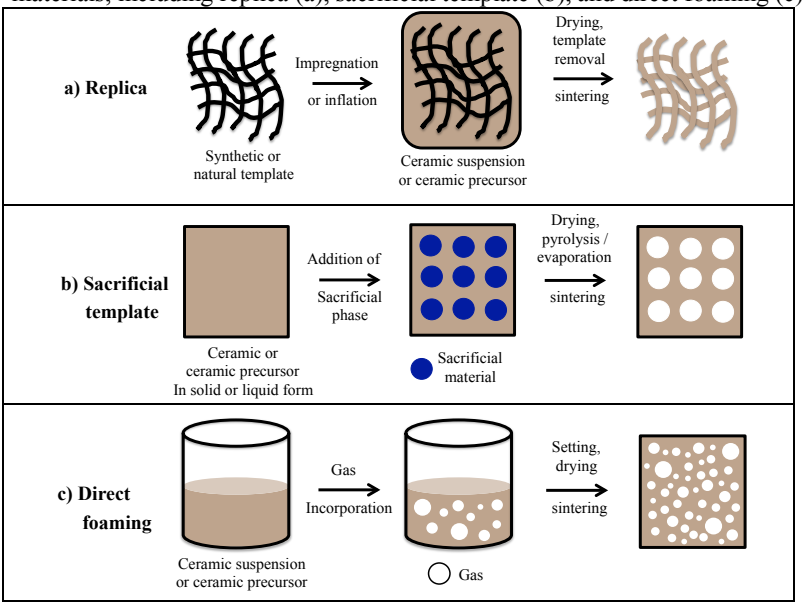

Source: Adapted from (Studart *et al.*, 2006).

In the present work, the sacrificial template technique was combined with extrusion to produce porous ceramic capillaries. The extrusion will be explained with more details in the subsequent item.

2.2 EXTRUSION OF CERAMICS

Shaping is a very important step in the manufacturing process of any material. This stage is responsible for determining the final geometry and function of the product. Moreover, it should associate the properties of the starting materials in a way that grants further steps of the manufacturing process to be completed successfully (Händle, 2007).

Examples of ceramic shaping processes are: dry pressing, extrusion, injection molding, and slip casting. Moreover, it is possible to separate the forming techniques into three different groups, according to the amount of water in the ceramic body. These groups are: dry shaping (0 – 5 wt% water), plastic shaping (18 – 25 wt% water), and liquid shaping (25 – 50 wt% water) (Lee e Rainforth, 1994; Händle, 2007).

Regarding to extrusion molding, it is a plastic shaping technique widely used in the traditional and technical ceramic industry. Throughout this processing method, complex shape parts can be produced at a high rate, reproducibility, and with narrow dimensional tolerance. (Isobe *et al.*, 2006; Boch e Niepce, 2007; Händle, 2007).

In general, this production technique consists of:

- choosing the suitable components that will yield the desired properties (flow, mechanical stability of the green bodies, debinding, and sintering);
- mixing powder into an aqueous/non-aqueous system until a homogeneous and stable paste is formed;
- forging the plastic mixture in the cavity of a mold; drying the extruded part in a controlled environment;
- debinding/sintering the green body in order to consolidate and densify the walls.

Therefore, the complete process can be divided into four main steps: materials selection; paste preparation; extrusion; and extraction of organic shaping additives (Boch e Niepce, 2007).

The first step consists of choosing appropriately the ceramic powders and the aqueous and/or organic phase. It is important to select wisely the ceramic powders once the shape and the size distribution of their particles play an important role in densification. On the other hand, the aqueous and/or organic phase should provide to the mixture paste an appropriate rheological behavior and a homogenous settlement of the ceramic particles during the extrusion (Boch e Niepce, 2007).

The second step comprises of dispersing the ceramic powder in the aqueous/non-aqueous system. It is important that the temperature of the ceramic suspension should fall in the range where the solvent is kept in liquid state throughout the whole mixing process (Deville, 2008). During this step, a homogeneous ceramic paste must be produced. This means a paste without agglomerates and with a large volume concentration of ceramic parts. Different additives may be used in order to help producing this homogenous paste: dispersants, binders, plasticizers, and lubricants (Boch e Niepce, 2007).

The third step consists of giving rise to the extruded part. In this stage, the homogenous paste is pushed through a shaped (or profiled) opening, also known as the extrusion die, using a piston or a screw Figure 3. After passing through the die, a shaped material with a constant cross-section is formed and then cut into desired pieces for further processes (Boch e Niepce, 2007; Händle, 2007).

Figure 3: Examples of the two predominant types of extruders: A) piston, B) screw.

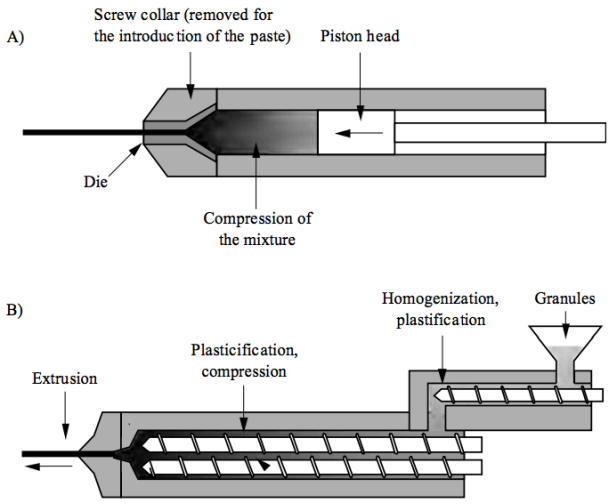

Source: (Boch e Niepce, 2007)

Finally, the green porous body is dried up and conducted to a thermal treatment to enhance the mechanical stability. Due to the amount of organic material added to the paste, it is recommended to make a special thermal debinding or burnout process to volatilize organics and avoid further defects such as cracks. Then, the sintering step should be carefully chosen to prevent excessive melting and at the same time to increase the mechanical strength (Boch e Niepce, 2007; Deville, 2008).

Shaping by extrusion has been reported in the literature to be suitable for a variety of ceramic materials. For instance, honeycombs made of extruded silicon carbide and cordierite (Colombo, 2005), and porous capillaries made of zirconia have been produced (Kroll *et al.*, 2010).

2.3 SURFACE FUNCTIONALIZATION AND CLICK CHEMISTRY

Surface plays a very important role in materials properties. For instance, the performance and behavior of materials can be dictated by the surface properties (Treccani *et al.*, 2013). Surface functionalization can be extensively explored to tailor surface and interface properties such as: wettability, biocompatibility, electrical conductivity, corrosion

resistance, and others. As a consequence, the surface's properties affect the overall material properties and performance, for that, it has been found in the literature many different functionalization techniques and approaches which are widely used and applied (Kroll *et al.*, 2012; Treccani *et al.*, 2013). There are various functionalization techniques using either inorganic or organic modifiers, and biomolecules that can be used to ceramic materials, which does not depend on dimensions or geometries.

Surface functionalization can be grouped mainly into three main categories: physical, chemical, and biological. Physical functionalization consists of machine-aided processes such as grinding, polishing or laser treatments. Chemical surface modification comprises mainly in the modification of the composition, charge, and energy at the surface of a certain material. Now biological functionalization involves the attachment of biological entities such as biomolecules (e.g. enzymes), cells, bacteria, and viruses on a surface of the material. It is also possible to combine more than one functionalization method in order to introduce multiple functionalities on the same material. The combination of functionalization techniques has been widely explored and studied recently, for being attractive for the design of devices and functional surfaces with a higher degree of complexity and applicability (Kroll *et al.*, 2010; Treccani *et al.*, 2013).

The surface modification of inorganic substrates by attaching organic molecules to the surface is a promising reality to tailor the surface properties of a material. For instance, an organic molecule, like an enzyme, can be anchored to a surface by physical adsorption, covalent bonding, and entrapment. The stability of the attached molecule will depend on the interactions of forces. They can be weak non-specific forces, such as hydrogen bonds, van der Walls or hydrophobic interaction, but they can be strong forces like covalent bonds or even ionic bonds (Hanefeld *et al.*, 2009; Mohamad *et al.*, 2015).

In the literature, a surface functionalization approach often utilized in ceramic materials is the silanization. Using this technique, it generates surface functional groups on inorganic surfaces that can lead to covalent bonding. It has been reported that not only planar inorganic surfaces, but also porous materials, nanoporous membranes, and colloidal particles can be chemically modified using mild conditions of processing (Plueddemann, 1982; Treccani *et al.*, 2013).

A silane compound can be defined as a monomeric silicon-based molecule containing four elements. Once silicon, in the periodic table, lays in the same family as carbon, it is also possible to make four covalent

bonds with other atoms. When silicon is bonded to at least one carbon, the compound is called organosilane, but it also can be bonded to hydrogen, oxygen, or halogen atoms. Some derivatives formed combining different arrangement of atoms can be highly reactive and be used to make covalent bonds with other molecules or surfaces. The general structure of a functional silane coupling compound is illustrated in Figure 4 (Plueddemann, 1982; Hermanson, 2013).

Figure 4: General structure of a silane-coupling agent, which includes a functional or reactive group.

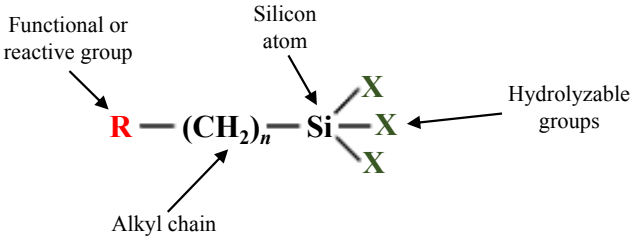

Source: Adapted from (Hermanson, 2013).

Silane reactive groups, shown in Figure 4, can covalently couple to certain inorganic substrates. Thus, it is possible to form bonds between an organic molecule with an inorganic surface such as some metal oxides (e.g. zirconia, alumina, and others). These metallic oxides can present highly compatibility with silanes displaying an efficient and stable surface modification. Usually, such ceramics present functional inorganic groups (hydroxyls) on their surface and these hydroxyls groups can react with the silanols on the silane coupling agent to form siloxane bonds. The complete coupling reactions between silane molecules and an oxide surface is shown in Figure 5 (Hermanson, 2013).

Figure 5: Silanization of ceramic surfaces. Reactions involved for an organosilane compound to an inorganic surface containing hydroxyl available groups.

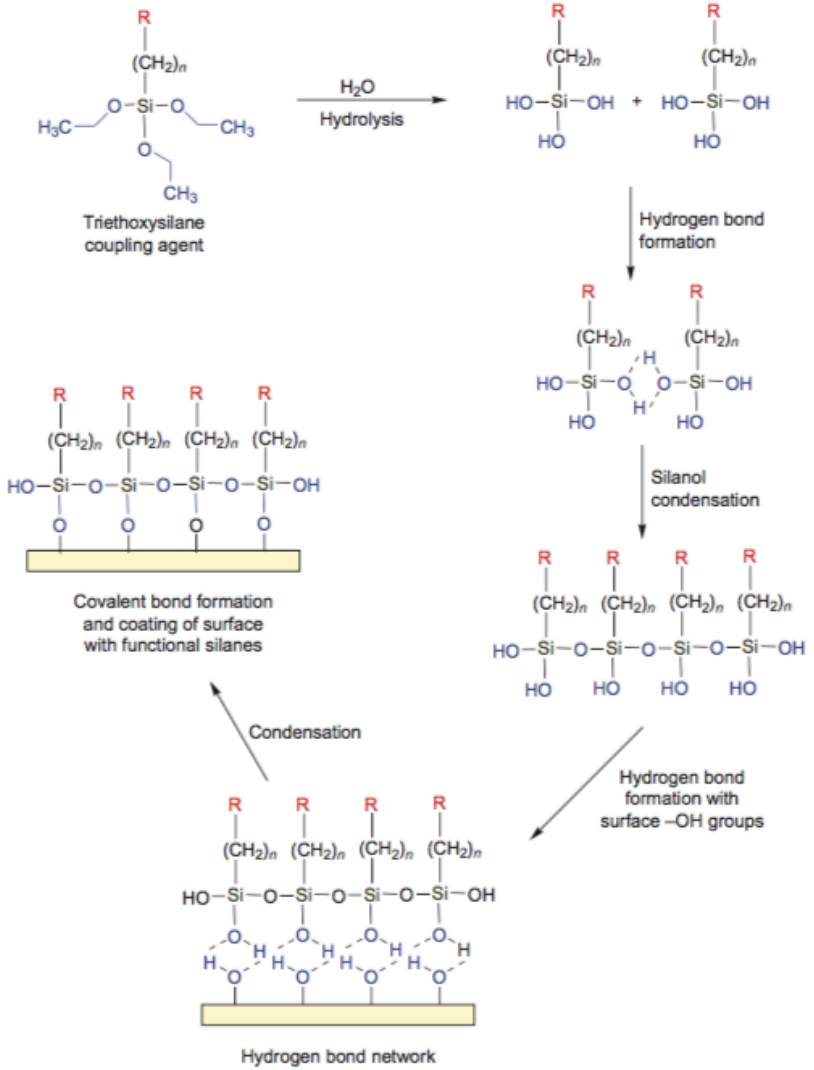

Source: (Hermanson, 2013).

As shown in Figure 5, the first step for the coupling of an organosilane compound to an inorganic surface involves the hydrolysis of alkoxysilane groups to generate reactive silanols. Afterwards, the

silanols undergo hydrogen bonding with other silanols forming a network of associated organosilane derivatives. Finally, some condensation reactions take place resulting in a polymerized coating on the surface of the substrate (Hermanson, 2013).

Organosilane precursors bearing functional groups such as amino, thiol, vinyl, cyanide, phenyl groups are commonly studied in the literature. For instance, it has been shown that silanes have been used to improve chemical bonding of zirconia for the immobilization of drugs and biomolecules, and in dentistry application (Treccani *et al.*, 2013). Usually, the mostly cited and employed silane precursors are aminosilanes (Kroll *et al.*, 2012; Treccani *et al.*, 2013). In particular, APTES, Figure 6, has been reported to often being used for cell adhesion and growth and enzyme immobilization.

Figure 6: Chemical structure of 3-aminopropyltriethoxysilane (APTES).

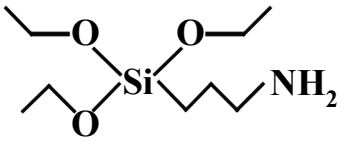

Source: Author.

The term “click chemistry” was coined by (Kolb *et al.*, 2001) and some strict criteria were established for a process to fit in this concept. For a reaction to be considered click chemistry, it should be a modular reaction wide in scope, produce inoffensive or no byproducts which can be easily removed, generate very high yields, and be stereospecific. Moreover, it should present simple reaction conditions, readily available starting materials, use of no solvent or the use of a benign solvent like water, and simple product isolation (Kolb *et al.*, 2001).

Click chemistry has been drawing attention in the scientific society because it presents advantages in the formation of a desired product connecting two molecular building blocks, in a very easy way, selective under mild processing conditions and with few or without byproducts (Moses e Moorhouse, 2007; Daugaard e Hvilsted, 2009; Castro *et al.*, 2016). It has been reported a rise in interest of click chemistry in biomedical research, such as discovery and tagging of biological systems with whole organisms, proteins, and nucleotides (Kolb e Sharpless, 2003).

A considerable number of reactions fit in the cited criteria; however, there is a very well-known example of click chemistry: the copper-catalyzed azide-alkyne cycloaddition (CuAAC), Figure 7. In this specific reaction, there is a formation of 1,4-disubstituted [1,2,3]-triazoles between a terminal alkyne and an aliphatic azide in the presence of copper (Castro *et al.*, 2016). Alkynes and azides groups are appealing coupling partners because they are inert towards biological molecules, easy to be synthesized, commercial available, and tolerant to many functional groups and reactions (Zilli, 2016).

Figure 7: Copper-catalyzed azide-alkyne cycloaddition (CuAAC) reaction as premier example of click chemistry.

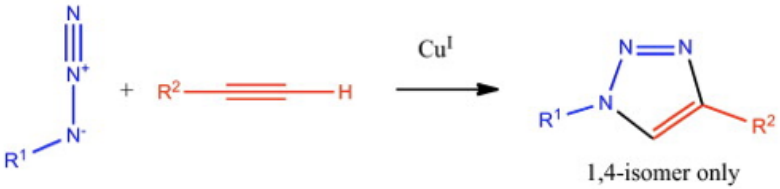

Source: Adapted from (Liang e Astruc, 2011).

2.4 ENZYMES

Enzymes are proteins, which they act as biological catalysts (Datta *et al.*, 2013). They are known as lock and key system and they are of great interest since they increase the rate of a reaction, are used in mild conditions of processing which make them interesting for industry. For instance, these biocatalysts can be used in the biofuel (Al-Zuhair *et al.*, 2011), paper (Bajpai, 1999), and food industry (Dieterich *et al.*, 2014). Moreover, enzymes can be used in the free or immobilized form (Datta *et al.*, 2013).

For instance, in food industry, the enzyme alcalase has been reported in the whey cheese production, where it leads to protein hydrolysis and the product of the enzymatic reaction used as a protein source for individual with reduced digestive capacity (Sousa Jr *et al.*, 2004). Another example, the biocatalyst papain has been used in the meat tendering industry, degrading the collagen and elastin, thus producing meat tenderness (Arshad *et al.*, 2016). Yet, the enzyme laccase has been cited in the juice processing business, working on the oxidation of phenolic compound in order to tailor the color and turbidity of the target juice (Kumar, 2015).

In food industry, it is common that protein hydrolysis is done in batch processes. In such processes, usually, large reactors are used where enzymes and substrates are poured in and mixed under constant temperature, controlled pH, and continuous stirring for several h. However it is difficult for batch regimes to keep a meticulous control throughout the entire process, therefore there is a variation of product properties, and huge amounts of high-priced enzymes are used only one time (Paulová *et al.*, 2013). However, in order to avoid losing the expensive enzymes during the process, they can be attached to a support (enzyme immobilization).

Enzyme immobilization is the confinement of enzyme to a phase (matrix/support), different from the substrate and product. In the literature, enzyme immobilization can be grouped into 4 different groups: physical adsorption, entrapment, covalent bonding, and cross-linking (Mohamad *et al.*, 2015). These immobilization approaches are schematically illustrated in Figure 8. Covalent biding of an enzyme to a solid support shows a powerful link between the system enzyme-support, minimizing the enzyme leaching during the process (Hanefeld *et al.*, 2009).

Figure 8: Examples enzyme immobilization: physical adsorption, covalent binding, cross-linking and entrapment.

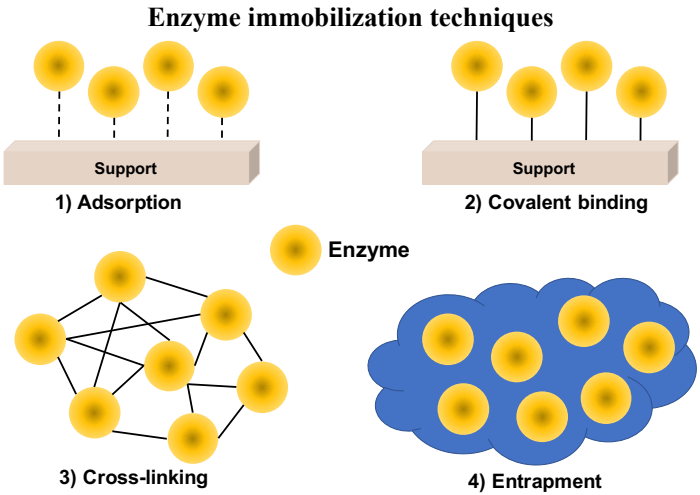

Source: Author.

2.5CHARACTERIZATION TECHNIQUES

2.5.1 Zeta potential

When ceramics particles are immersed in an aqueous medium, they normally acquire surface charges, which are influenced by the pH and electrolyte concentration of the solvent. Depending on the interaction among the charged particles, they might tend to disperse, aggregate or flocculate. Consequently, it is important to be familiar with the concept of zeta potential (Baptista e Lucas; Panalytical).

Analyzing Figure 9, the liquid layer surrounding the particle exists as two parts: an inner region that is called the Stern layer, and an outer region, which is called diffuse layer. In the Stern layer the ions are strongly bound to the particle; on the other hand, in the outer region the ions are less attached. Within the diffuse layer, there is a notional boundary where ions and particles form a stable entity. For instance, when a particle moves, some ions within the boundary move with it; however, there are some ions beyond the boundary, which do not travel with the particle. This boundary is called slipping plane, and the potential that exists at this boundary is known as the zeta potential (Baptista e Lucas; Panalytical; Pujala, 2014).

Figure 9: Zeta potential scheme.

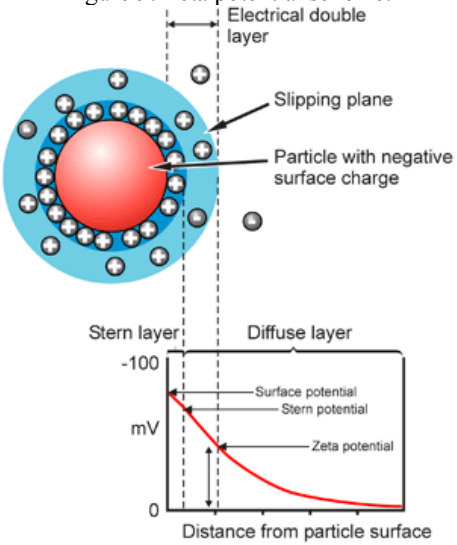

Source: (Panalytical)

The stability of a colloidal system can be estimated by the magnitude of the zeta potential. If all the particles in suspension have a large negative or positive zeta potential magnitude, then they will tend to repel each other and, therefore there is no tendency to occur aggregation or flocculation. On the contrary, if the particles have low zeta potential values, then there is no force to avoid the particles coming together and flocculating. Moreover, when a particle is electrically neutral at a given pH (zeta potential is equal to zero), this is point is known as the isoelectric point or IEP (Pujala, 2014). Figure 10 depicts the stability of a suspension varying the pH as well as it highlights the isoelectric point of a certain material (Pujala, 2014).

Figure 10: Example of a zeta potential titration of a gelatin as well as examples of possible interactions among particles.

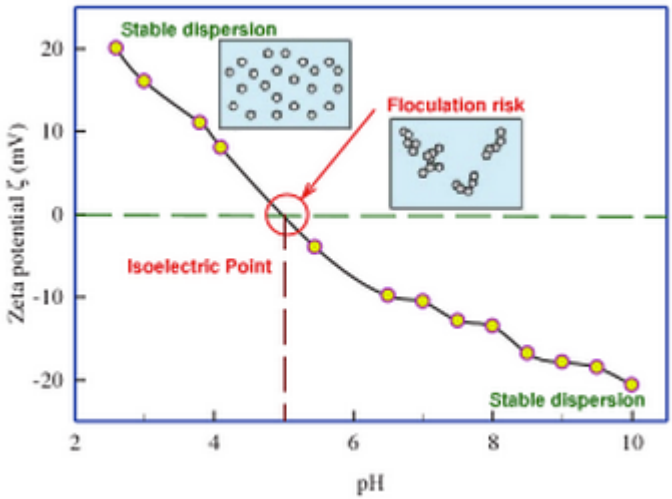

Source: (Pujala, 2014)

The boundary between stable and unstable suspensions is generally taken at either +30 mV or -30 mV. Particles with zeta potentials more negative than -30 mV or more positive than +30 mV are normally considered stable (Panalytical).

2.5.2 Bulk density and open porosity

Bulk density can be defined as the ratio between mass and external volume. Furthermore, the external volume takes into account all the pores, opened and closed, inherent to the mass of the material (Keulen, 1973). For the specific case of microtubes (e.g. capillaries), the bulk density, can be determined using the following equations (Eq.1 and Eq.2):

$$\rho_{bulk} = \frac{m}{V} \tag{1}$$

$$V = \pi\left(R_{outer}^2 - R_{inner}^2\right).h \tag{2}$$

where ρ_{bulk} is the bulk density (kg/m^3); m is the mass (kg); V is the volume (m^3); R is the radius (m); and h is the length (m) of the ceramic capillary.

Once determined the bulk density of the material and measuring its apparent density (density that takes into account the volume of compact solid material and of closed pores, excluding the volume of open pores). The open porosity can be determined using the following equation (Liu e Chen, 2014):

$$\theta = \left(1 - \frac{\rho_{bulk}}{\rho_s}\right).100\% \tag{3}$$

where θ stands for the open porosity; ρ_{bulk} for the bulk density; and ρ_s for the apparent density (Liu e Chen, 2014).

In pursuance of determining the theoretical total porosity of the samples, some assumptions are made. For example, it is supposed that all the additives (decane, beeswax, and stearic acid) in the ceramic paste would lead to porosity and all the expansion and contraction throughout the process were neglected. So, the theoretical open porosity equation is shown below:

$$\theta_{theoretical} = \left(1 - \frac{V_{zirconia}}{V_{zirconia} + V_{additives}}\right).100\% \tag{4}$$

where $\theta_{theoretical}$ stands for the theoretical open porosity; $V_{zirconia}$ for zirconia volume; $V_{additives}$ for the volume of additives used in the composition of the ceramic capillaries.

The volumes were estimated dividing the mass of the component by its apparent density.

2.5.3 Mercury intrusion porosimetry

The mercury intrusion porosimetry is a widely used and convenient characterization technique for detecting pores in the range from about 500 μm up to 2 nm. Additionally, mercury intrusion porosimetry delivers a broad range of information such as total amount of pores, total pore volume, pore size distribution, specific area of a sample, and bulk and skeletal density (Giesche, 2006; Kaufmann, 2017).

In this technique, mercury is employed due to its high contact angle, between 112° and 142°. Thus, it does not wet most materials and it is considered a non-wetting agent; it presents low chemical reactivity with most materials at room temperature; and it has high surface tension (≈ 0.48 N/m) (Kaufmann, 2017). As a consequence, pores within a material cannot spontaneously absorb mercury. Nevertheless, this reluctance to penetration can be overcome by applying an external pressure. Such external pressure should exceed the surface tension of mercury and the contact angle between mercury and material. Moreover, the required pressure depends on the pore size, assuming the pores to be cylindrical (Webb, 1997; Giesche, 2006; Kaufmann, 2017):

$$p = -\frac{2\gamma cos\alpha}{r} \tag{5}$$

where p is the absolute applied pressure; γ is the surface tension of mercury; α is the contact angle between the mercury and solid; and r is the pore radius (Giesche, 2006; Kaufmann, 2017).

2.5.4 Nitrogen adsorption isotherms and BET model

Adsorption can be defined as the adhesion of molecules, ions or atoms to a surface. Throughout this adhesion process a film of the adsorbate is built on the surface of the adsorbent. The adsorption process is usually studied through graphs known as adsorption isotherms. These graphs display the relation between the amount of adsorbate adsorbed on the surface of the adsorbent and pressure, under isothermal conditions. Freundlich, Langmuir, and BET theory are typical models for interpretation of the measured adsorption isotherms (Epa; Learning, 2009).

In 1938, Brunauer, Emmett and Teller elaborated the initial version of a model, which thereafter would be granted with their names (Brunauer-Emmett-Teller or BET model). The proposed isotherm equation was a generalization of the Langmuir's theory and elucidates the multilayer adsorption of gases (Brunauer *et al.*, 1939). As the Langmuir isotherm takes into account only monolayer adsorption, it is not an accurate representation of how nitrogen actually adsorbs to the surface. Indeed, a better approximation for this process is to use the BET model, which is based on the possibility of multilayer adsorption and assumes that each multilayer follows the Langmuir isotherm with no interaction among the multilayers (Brunauer *et al.*, 1939; University, 2011).

Plotting the experimental data in the range of low pressures, according to the low p/p_0 simplified BET isotherm equation Eq. 6, gives a straight line; from which the regression coefficients provides an estimation of the monolayer volume (v_m) (Brunauer *et al.*, 1939; Wikipedia, 2017).

$$\frac{1}{\left(1 - {}^{p}/_{p_0}\right)} = \frac{v}{v_m} \tag{6}$$

where p stands for the pressure measured in equilibrium; p_0 for the initial system pressure; v for the total adsorbed gas; and v_m for the adsorbed gas volume when the solid surface is completely covered by a monolayer.

In addition, the monolayer volume enables the calculation of the number of gas molecules necessary for the total covering of the adsorbent surface with a monolayer; thus, multiplying the obtained value by the molecular cross-sectional area (obtained from the density of the solidified gas or of the liquefied gas) gives an estimate of the adsorbent surface area, Eq. 7 (Brunauer *et al.*, 1939; Wikipedia, 2017).

$$S = \frac{v_m L_{av} A_{ad}}{M_v} \tag{7}$$

where v_m is the monolayer volume explained previously; L_{av} is the Avogadro number; A_{ad} is the adsorbate molecular cross-sectional area; and M_v is the volume occupied by 1 mol of the adsorbate molecule.

3 MATERIALS AND METHODS

To produce porous ceramic capillaries, yttria-stabilized zirconia powders TZ-3Y-E and TZ-3YS-E with mean particle diameters of 40 nm and 90 nm, respectively, beeswax, stearic acid, decane and hexane were used as the starting materials.

For the surface functionalization of the capillaries, (3-aminopropyl)triethoxysilane (APTES), dimethylformamide (DMF), 3-bromopropionic acid, hydroxysuccinme (NHS), N-(3-dimethylaminopropyl)-N-ethylcarbodiimide (EDC), and the sodium azide (NaN_3) were used.

Albumin from chicken egg white (BSA) was used as the protein and pure subtilisin A (protease from *Bacillus licheniformis,* E.C. number: 3.4.21.62) was employed as the enzyme. Subtilisin A was chosen as the selected enzyme, based on a previous worked published by Sewczyk *et al*., where it displayed promising results regarding to the breakdown of casein (Sewczyk *et al.*, 2018). For the acetylene functionalization of proteins, 4-pentynoic acid, EDC, and 2-(N-Morpholino)ethanesulfonic (MES) were utilized. While for the click chemistry, MES and copper sulfate, and ascorbic acid were the raw materials for that purpose.

All materials that have been used throughout this work with manufacturers and other details are given in Chart 1.

Chart 1: Information about the starting materials according to the manufacturer data.

Material	Manufacturer	Details
4-pentynoic acid	Sigma-Aldrich	CAS # 6089-09-4
APTES	Sigma-Aldrich	Lot # SHBG1799L
Beeswax white	Carl Roth	Charge: 146239798
BSA	Sigma-Aldrich	Lot # SLBK0389V
Casein	Sigma-Aldrich	Lot # BCBQ8633V
Copper sulfate	Carl Roth	Charge: 246240190
Decane	Sigma-Aldrich	Anhydrous
DMF	Sigma-Aldrich	Lot # STBC7710V
EDC	Sigma-Aldrich	Purum
Fast-curing silicone	BEGO	Lot # 1422240145
Folin & Ciolcaltea's reagent	Sigma-Aldrich	Lot # BCBR9547V
HCl	Sigma-Aldrich	1 M
L-ascorbic acid	Sigma-Aldrich	Anhydrous
MES hydrate	Carl Roth	Charge: 186243837
n-Hexane	Sigma-Aldrich	Anhydrous
NaOH	Sigma-Aldrich	1 M
Orange II sodium salt	Sigma-Aldrich	Dye content ≥ 85 %
Potassium phosphate	Sigma-Aldrich	Lot # WXBC1644V
Subtilisin A	Sigma-Aldrich	Activity: 7-15 U/mg
Sodium azide	Sigma-Aldrich	ReagentPlus
Sodium carbonate	Sigma-Aldrich	Lot # SZBF1480V
Stearic acid	Sigma-Aldrich	Grade I
TCA	Sigma-Aldrich	Lot # SLBR2137V
ZIRCONIA TZ-3Y-E	TOSOH	Particle size of 40 nm
ZIRCONIA TZ-3YS-E	TOSOH	Particle size of 90 nm

Source: Author.

The whole process of sample preparation can be divided into three groups: ceramic paste preparation (blue), ceramic processing (red), and as well as surface functionalization and click chemistry (yellow), as shown in Figure 11.

Figure 11: Flowchart displaying the processing route for the fabrication of porous ceramic capillaries with enzymes immobilized on it.

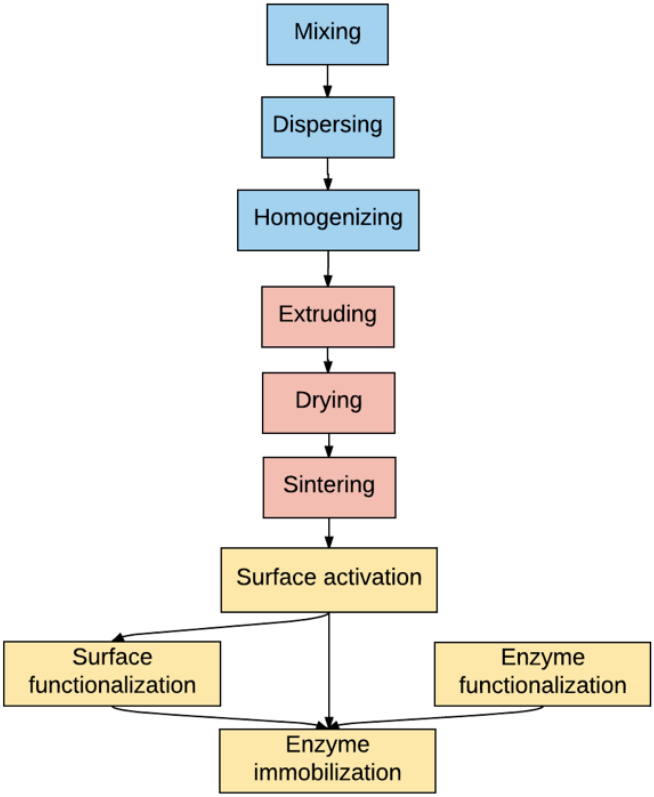

Source: Author.

3.1 CERAMIC PASTE PREPARATION

In pursuance of fabricating porous microtubes, 40 g of decane were heated up to 353K in a beaker using a heating plate, and, subsequently, 28 g of beeswax and 3 g of stearic acid were added to the organic solvent and stirred until a homogenous solution was reached. Thereafter, 300 g of zirconia powder were added to the solution. It was mixed quickly with a glass rod prior to the dispersion of ceramic particles with an ultrasonic horn (Heinemann, Germany; Brason Sonifier 450) for 5 min at 240 W and a pulse rate of 0.5. To influence the porous properties of the capillaries, three different ceramic powder compositions were used for paste preparation: (1) YSZ TZ-3Y-E, (2) YSZ TZ-3YS-E, and (3) a mixture of

1:1 (w/w) from both powders. For the complete homogenization of the ceramic paste and evaporation of the remaining hexane, the ceramic suspension was mixed using a high speed dispermat LC2 (Getzmann VMA, Germany; LC2) for 35 min at 353 K (Kroll *et al.*, 2010).

3.2 CERAMIC PROCESSING

Once a stable ceramic paste was produced, it was placed in a temperature controlled double wall container. The container was closed and sealed with a pressing piston. Prior to extrusion, the suspension was held inside the vessel for 2 h and 30 min at 313 K to reach a homogeneous ceramic paste temperature. The direct extruder, shown in Figure 12, consisted of: an extrusion die with 1.6 mm of diameter and an integrated pin with 1.0 mm of diameter; a spindle drive with shaft joint connected to the pressing piston, which was used to control the extrusion force by a load cell; a conveyor belt, on which extruded defect-free green capillaries were transported at controlled speed.

Figure 12: Schematics of the piston extruder used to produce porous ceramic microtubes.

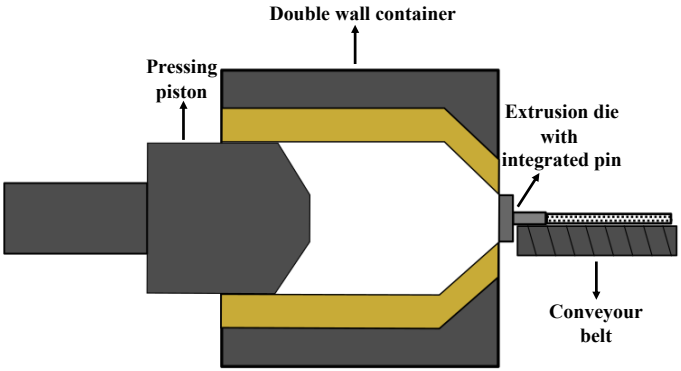

Source: Author.

After the tubes were extruded, they were dried for at least 48 h, at room temperature, and a relative humidity of approximately 45 %. Subsequently, the capillaries were debinded and sintered, using the sintering program shown in Table 1. This thermal program was used taking into account previous published work on porous microtubes made of zirconia (Kroll *et al.*, 2010). Finally, the pieces were cut in 2 different lengths: 25 mm and 100 mm.

Table 1: Debinding and sintering route.

Segment	Temperature (K)	Heating rate (K/h)	Dwell time (h)
1	298 → 578	180	0.5
2	578 → 798	30	1
3	798 → 1348	120	2
4	1348 → 298	-300	-

Source: Author.

3.3 SURFACE FUNCTIONALIZATION AND CLICK CHEMISTRY

3.3.1 Hydrothermal activation

Prior to the silane functionalization, the sintered capillaries were activated by hydroxylation using a hydrothermal treatment, an autoclave (Systec GmbH, Germany; Systec VX-100). This step plays an important role, since OH groups are created on the surface of the ceramic microtubes, Figure 13, and, subsequently, they bond to the hydrolyzed silane coupling agent. For this hydrothermal activation, the samples were placed in an autoclave with the following parameters: sterilization temperature of 394 K for 20 min and drying at 393 K for 10 min (Kroll *et al.*, 2012).

Figure 13: Hydroxylating the surface of the porous ceramic substrate.

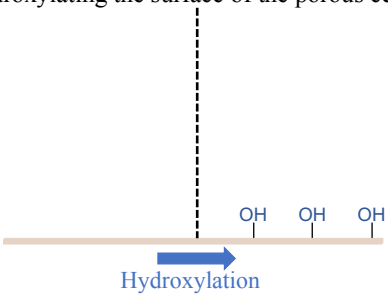

Source: Author.

3.3.2 Silane (APTES) functionalization

The process of functionalization with a silane is also known as silanization, in which the silane group is bonded to the surface that contains hydroxyl groups, Figure 14. Three types of silane depositions using APTES as the aminosilane were tested and described hereafter.

Figure 14: Silane functionalization using APTES on a hydroxylated surface.

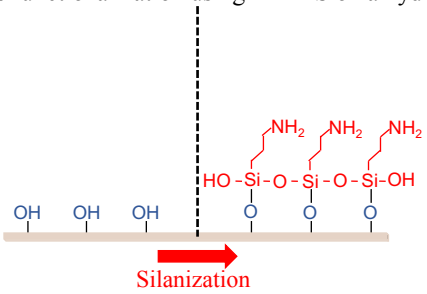

Source: Author.

3.3.2.1 APTES organic solvent deposition

In this approach, the activated capillaries were immersed in toluene (0.05 g/mL), and treated in an ultrasonic bath for 5 min. Afterwards, they were placed into a two-neck round-bottom flask and heated up to 383 K using an oil bath. APTES was added to the organic solvent, in a ratio of 5 µL of APTES for each mL of solvent. With the aid of a reflux, the mixture was stirred for 6 h. In the first 20 min, it was stirred under a flux of nitrogen gas. Afterwards, the capillaries were washed with toluene and distilled water and dried at 343 K for at least 24 h (Zilli, 2016).

3.3.2.2 APTES aqueous deposition

In this procedure, a 0.2 M solution of APTES in double-deionised water was prepared. In addition, 12 hydroxylated capillaries of 25 mm length were immersed in 10 mL of these fresh silane solution and they were incubated in a thermal shaker (Heidolph Instruments GmbH & Co. KG, Germany; product Unimax 1010) at 338 K and 150 rpm for 24 h. After incubation, the samples were thoroughly cleaned using distilled water until a neutral pH was reached and dried at 343 K for at least 24 h (Hermanson, 2013). In the case of the samples with 100 mm length, 3

pieces were immersed in 10 mL instead of 12, to keep the same ratio as before.

3.3.2.3 APTES aqueous/organic solvent deposition

In this method, a 0.2 M APTES solution was prepared inin a mixture of 3% double-deionised water in ethanol (v/v). Tweleve hydrothermally activated microtubes of 25 mm length were immersed in 10 mL of this fresh silane solution and they were incubated in a thermal shaker at room temperature and 150 rpm for 24 h. Afterwards, the sample was thoroughly cleaned using distilled water until reaching a neutral pH and dried at 343 K for at least 24 h (Hermanson, 2013).

3.3.3 Azide functionalization of amino modified zirconia capillaries

The obtained amino-modified zirconia ceramic capillaries were immersed in DMF in a ratio of 800 mg of capillaries to 20 mL of solvent. In a two-neck round-bottom flask, 0.56 g of 3-bromopropionic acid, 0.48 g of NHS, and 0.8 g of EDC were added to the capillaries in DMF, and it was left stirring under reflux, light protection, and nitrogen gas flux at 353 K for 24 h. Afterwards, 0.6 g of sodium azide was added to the mixture and it was left at unaltered conditions for additional 24 h. At last, the ceramic capillaries with azide groups (Figure 15) were washed 3 times with DMF and water, and dried at 343 K for at least 24 h (Zilli, 2016).

Figure 15: Azide functionalization.

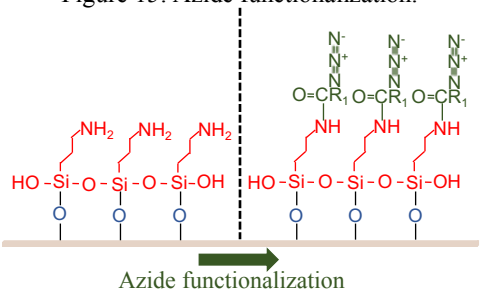

Source: Author.

3.3.4 Acetylene functionalization of protease

Protease from *Bacillus licheniformis* was functionalized with acetylene groups (Figure 16) as preparation for the click reaction with the azide groups on the ceramic capillaries. Therefore, a solution of 1 mg of the enzyme in 1 mL of 10 mM MES buffer (pH 5.5) was prepared. For each 2 mL of this solution, 50 µL of 0.1 M 4-pentynoic acid (aqueous solution) was added and vortexed for 2 min. In the next step, the solution was placed in an ice bath for 15 min. Subsequently, 1 mg of EDC was added to the mixture and vortexed for 2 min, and stored in the ice bath for additional 4 h. Finally, the solution was dialyzed using dialysis tube at 277 K for 24 h in a 0.1 M sodium phosphate buffer. The dialysis buffer solution was changed every 3 h. After the dialysis the protein solution was kept at 277 K for further use in click chemistry (Zilli, 2016).

Figure 16: Acetylene functionalization of proteins.

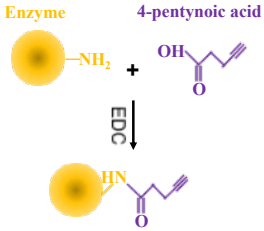

Enzyme functionalization

Source: Author.

3.3.5 Click reaction of azide functionalized capillaries and acetylene functionalized protease

Since the capillaries were functionalized with azide groups and the enzymes with acetylene groups, a specific reaction (click chemistry) between the modified microtubes and proteins was feasible (Figure 17). In this step, azide-functionalized capillaries were immersed in 10 mM MES buffer solution (65 mg of ceramic capillary in 2 mL of MES). To this solution, an aliquot of 175.0 µL of acetylene-modified protein (subtilisin A) was added and vortexed for one min. Afterwards, 10 µl of 0.2 M ascorbic acid and 10 µL of 0.1 M copper sulfate were added to the mixture and vortexed for one min. The sample was placed in a shaker at 277 K, 400 rpm, and for 16 h (Gole e Murphy, 2008; Zilli, 2016).

Figure 17: Click chemistry of the functionalized microtube with the functionalized protease.

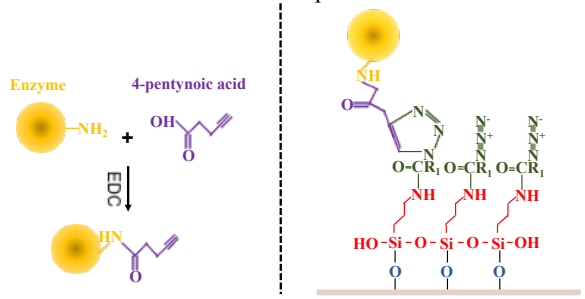

Source: Author.

3.4 CHARACTERIZATION

3.4.1 Powder characterization

Zirconia TZ-3Y-E and TZ-3YS-E powders were first characterized using a scanning electron microscope (Carl Zeiss Oberkochen, Germany; DSM 940A) to assess its morphology and particle size; dynamic light scattering (Malvern Instruments Ltd, England; Zetasizer nano) was used to evaluate the particle size distribution, as well as the colloidal stability (zeta potential titration); the apparent density of the powders was determined by helium pycnometry (POROTEC GmbH, Germany; Pycnomatic ATC); BET (Bel Japan Inc., Japan; Belsorp-Mini II) was used to assess the surface area of the powders.

Preceding the SEM analysis, the YSZ powders were placed on a carbon tape and, afterwards, sputtered with gold (Judges Scientific plc, United Kingdom; K550). For the particle size distribution and zeta potential titration, a 0.05 wt% solution of zirconia in deionized water was prepared and the particles dispersed in an ultrasound bath for 30 min. NaOH and HCl 1M, were used as the base and acid, to shift the pH of the solution.

The nitrogen adsorption-desorption isotherms for the studied material were conducted at 77 K in a volumetric gas adsorption instrument (Bel Japan Inc., Japan; Belsorp-Mini II) and the specific surface areas were calculated using the BET method. About 50 mg of the samples were degassed for 16 h at 293 K under reduced pressure (< 2

mbar) and subsequently exposed to an argon atmosphere at room temperature for thirty min prior to the analysis. Further procedural information, so as an overview of the standard methodology, can be found in the IUPAC recommendations (Sing *et al.*, 1985; Rouquerol *et al.*, 1994).

3.4.2 Structural characterization

The structural characterization consisted of a series of material characterization such as scanning electron microscopy; optical microscopy; bulk density and open porosity based on the geometry and weight of the specimens; mercury intrusion porosimetry; and nitrogen adsorption isotherms and BET model.

Scanning electron microscope images were acquired from one sample of each formulation. Representative pieces were taken from the radial width of the specimen und they had their length cut with a scalpel in order to have a suitable size for the analysis.

Cross sectional pictures of the ceramic microtubes were taken before and after sintering using an optical microscopy (Keyence Corporation of America, United States of America; VHX-600DSO) to assess their shrinkage and density. Therefore, the outer and inner diameter of ten samples of each material type were measured using the software of the optical microscope.

In order to determine the bulk density of the specimen, 10 samples of each formulation type were dried at 343K for 24 h. Afterwards, they were separated and, specifically, labeled. Four measurements of the diameter were taken using a software, its length was measured (Mitutoyo digital caliper), and the mass of the samples was measured using a precision scale.

Once calculated the bulk density and measuring the apparent density of the specimens, Eq. 3 was used to estimate the open porosity.

For the intrusion analysis, representative pieces were taken from the middle of the length of the specimen and carefully cut with a scalpel in order to have suitable size for porosimetry equipment (Porotec GmbH, Germany; Pascal – Porosimeter).

The nitrogen adsorption-desorption isotherms for the studied material was described previously.

3.4.3 3-point bending test (3PB) and Weibull distribution

The flexural strength of the porous ceramic capillaries was measured using a universal testing machine (Zwick GmbH & Co. KG, Germany; Proline tabletop testing machines Roell Z005). The 3-point bending tests were conducted according to the standard DIN EN 843-1 (Advanced technical ceramics - Mechanical properties of monolithic ceramics at room temperature Part 1: Determination of flexural strength) (Normung, 2008).

It is reported in the literature that the 4-point bending test presents more reliable data regarding to the tested material, because the total volume of the tested specimen under high stress is more representative when compared to the 3-point bending test (Quinn *et al.*, 2009). However, in the present work, the 3-point bending test was chosen instead of the 4-point bending test, in order to compare the measured results with previous works (Kroll *et al.*, 2010; Werner *et al.*, 2014), and due to its easy measurement setups and absence of complication in sample preparation (Seeber *et al.*, 2013)

For the 3-point bending test, capillaries of 12 mm length were fixed on support rollers which had a distance of 8 mm (L). Moreover, the universal testing machine was equipped with a load cell for 5 kN, and the velocity applied was 0.4 mm/min. From each formulation, 30 samples were tested for statistical significance. The flexural strength was calculated using the following equation:

$$\sigma_f = \frac{8.F.L.OD}{\pi.(OD^4 - ID^4)} \tag{8}$$

where σ_f is the flexural strength; F, measured force at fracture; L, the distance between support rollers; OD, outer diameter, and ID, inner diameter.

The acquired data ware further analyzed using the Weibull distribution, where the characteristic flexural strength and the Weibull modulus were determined for each formulation type. The Weibull distribution is commonly applied for characterizing mechanical strength of brittle ceramics with defects based on the weakest defect principle (Weibull, 1951).

3.4.4 Water permeate flux test

Since it is expected that varying the staring particle size and introducing beeswax as a sacrificial template for the specimen would lead to changes in its structure; it is interesting to investigate the effect of these changes on the water permeability properties of the produced capillaries. A sketch of the used measurement system is shown in Figure 18.

Figure 18: Schematics of the water flow equipment used for permeability of the porous ceramic structure.

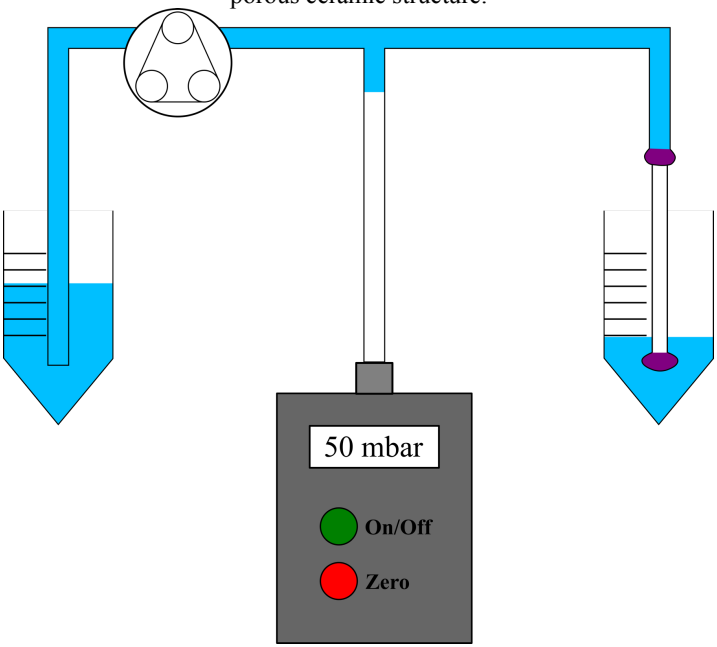

Source: Author.

In order to assess the water permeate flux, sintered capillaries with length of 100 mm were operated in a dead-end mode. To do so, one end of the ceramic tube was sealed with a fast-curing silicone (silicone duplicating material), while the opposite side was connected to a silicon tubing, also sealed with the fast-curing silicone. The silicon tubing was connected to a T-junction connector, where one outlet was attached to a digital manometer (Comark Instruments, United Kingdom; C9500) and the other to a peristaltic pump (Ismatec Cole-Parmer GmbH, Germany; BVP standard).

For this test, double-deionized water was used as feed solution and pressures ranging from 25 to 500 mbar were used (25, 50, 75, 100, 200, 300, 400, and 500 mbar). For each chosen pressure, the test ran ten min, and, subsequently, the collected water was weighed in a precision scale. Three samples of each capillary formulation type were tested for statistical significance.

3.4.5 Quantification of amino groups

In order to quantify the APTES molecules bonded to the ceramic capillary, a photometric acid orange II assay was employed (Kroll *et al.*, 2010). In this characterization method, three 25 mm microtubes of different compositions were individually placed in a 2 mL Eppendorf tube. These Eppendorf tubes were filled with 1.75 mL of a 0.5 mM orange II sodium salt solution in HCl (pH 3). The samples were shaken at 294 K and 1100 rpm, in the dark for 24 h.

Afterwards, the capillaries were washed three times with HCl (pH 3) and, individually, they were stored in 2 mL Eppendorf tubes filled with 2 mL of NaOH (pH 12). Once again, the tubes were shaken at 294 K and 1100 rpm, in the dark, for 15 min. Prior to the photometric measurement, the sample solution was diluted using NaOH (ph 12), using the ratio 1:3. The quantitative estimation of amino groups were assessed by photometric measurement at the wavelength of 483 nm in triplicates.

To evaluate the number of amino groups bonded to the porous ceramic microtubes, firstly, a calibration curve was made, relating the intensity and quantity of the orange salt II dye. Figure 19 shows the built calibration curve and from it, it is possible to obtain a linear relation between intensity and quantity of the dye:

$$A = 9.9267d - 0.0287; R^2 = 0.9939 \quad (9)$$

where A is the measured absorbance intensity; d, the quantity (in μg) of the die; and R^2, the coefficient of determination.

Therefore, from the equation, it is possible to estimate the quantity of the dye, thus the number of amino groups attached to the ceramic capillary.

Figure 19: Calibration curve for the photometric acid orange II assay relating absorbance intensity and dye quantity.

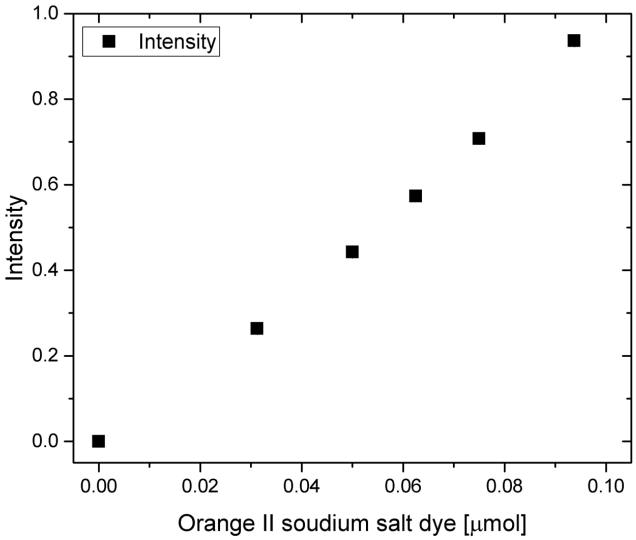

Source: Author.

3.4.6 Enzyme activity under batch and flow conditions

One way to investigate the proposed accomplishment of all functionalization steps (APTES deposition, azide functionalization, and acetylene functionalization of protease) combining with the click chemistry was performing a protease activity assay. For instance, in this assay, just hydroxylated capillaries with immobilized protease, for control group, and full functionalized ceramic microtubes with immobilized subtilisin A were used.

The activity of the immobilized protease from *Bacillus licheniformis* was determined following the protease activity assay protocol as described subsequently. Casein was used as substrate (Cupp-Enyard, 2008) under batch and flow regime, depicted in Figure 20. Basically, the protocol can be divided into 3 steps: preparation of the reagents, setting up the protease assay, and calculation of the enzyme activity.

Figure 20: Schematics of the enzyme batch (left side) and flow (right side) activity test.

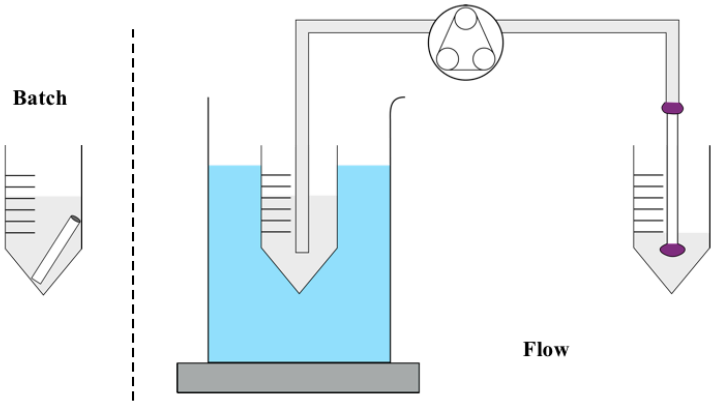

Source: Author.

3.4.6.1 Preparation of reagents for enzyme activity determination

The following reagents are used (Cupp-Enyard, 2008):

- A 50 mM potassium phosphate buffer solution at pH 7.5. To prepare it, 11.4 mg/mL of potassium phosphate dibasic trihydrate was dissolved in purified water and pH was adjusted with a 1 M HCl solution. The buffer solution was heated up to 310 K prior to using.
- A 0.65 % weight/volume casein solution. This was done by mixing 1.625 mg of casein from bovine milk, in 250 mL of the 50 mM phosphate buffer solution. The solution temperature was gradually raised under gentle stirring up to 353 – 358 K for about ten min, until a homogenous dispersion was reached. The dispersion should not reach the boiling point. If necessary, after the dispersion procedure, the pH was readjusted with NaOH or HCl until reaching a pH of 7.5.
- A 110 mM trichloroacetic acid solution (TCA). It was prepared by diluting a 6.1 N TCA stock solution with purified water in a ratio of 1:55.
- A 0.5 M Folin & Ciolcaltea's reagent. This phenol reagent is the solution that will react with tyrosine to generate further measurable color shift, which will be directly related to the activity of proteases.

- A 500 mM sodium carbonate solution. It was produced using 53 mg/mL of anhydrous sodium carbonate in purified water.
- A 10 mM MES buffer solution.

3.4.6.2 Setting up the protease assay (Batch)

For the enzyme activity test under batch condition, four "clicked" capillaries of 25 mm of each formulation were used. Glasses vials of 15 mL were employed in this test. Five mL of the casein solution were pipetted in the empty vial glass, and they were put inside the thermal shaker at 310 K for 5 min. Meanwhile, the enzyme immobilized microtubes were washed with the 50 mM potassium phosphate buffer three times. Later, the capillaries were added each for each glass and incubated at 310 K for 10 min. The enzyme activity and posterior release of tyrosine (which is the product of the enzymatic activity) during this incubation time and condition is what will be further measured and compared.

Then, the functionalized tubes were removed from the vials, 5 mL of the TCA solution were pipetted to each vial to stop the reaction, and, once again, the samples were incubated for 30 min at 310 K. Concurrently, the capillaries were washed with the 10 mM MES buffer solution 3 times, and stored in 2 mL Eppendorf tubes filled with 2 mL of the MES solution at 277 K.

Subsequently, the casein-TCA solutions were filtered using 0.45 μm polyethersulfone syringe filters. 2 mL of this filtered solution were added to another new glass vial. 5 mL of sodium carbonate, were added and immediately, 1 mL of the 0.5 M Folin & Ciolcaltea's reagent was joined in every glass container. Thereafter, the samples were incubated at 310 K for 30 min.

Finally, the solutions were filtered again, using the 0.45 μm polyethersulfone syringe filter, 200 μL of this filtered solution were added to 96-well plates in triplicate for further spectro-photometric measurements at the wavelength of 660 nm.

For the sake of assessing the stability of the enzymes on the ceramic porous substrates, by means of the quantity of tyrosine released, they were conducted to the same assay up to 6 times. Doing so, the enzymes were susceptible to the leaching process promoted by the washing steps used in the protocol.

3.4.6.3 Setting up the protease assay (Flow)

For the analysis of enzyme activity test under flow condition, four functionalized capillaries of 100 mm length of each formulation were tested. 30 mL of casein solution was added to a Falcon tube in a water bath at 310 K. Moreover, the casein solution was pumped into the "clicked" tubes, working in a dead-end mode. The casein flow was adjusted until reaching a flow rate of 0.2 mL/min and stabilized in this condition for at least ten min prior to collecting the samples for the assay (Kroll *et al.*, 2012). Samples were collected each ten min of test (after 10, 20 and 30 min of running test). Approximately 2 mL of solution was collected for each sample after 10 min. Then, 2 mL of the TCA solution were pipetted to the vial and the samples were incubated at 310 K for 30 min.

Afterwards, the casein-TCA solutions were filtered using 0.45 µm polyethersulfone syringe filters. Two mL of this filtered solution were cast to another new glass vial. Five mL of sodium carbonate, were added and forthwith, 1 mL of the 0.5 M phenol reagent was joined in each container. Next, the samples were incubated at 310 K for 30 min.

Lastly, the solutions were filtered again, using the 0.45 µm polyethersulfone syringe filter, 200 µL of this filtered solution were pipetted to the UV plate in triplicate for further spectro-photometric measurements at the wavelength of 660 nm.

3.4.6.4 Calculation of the enzyme activity

The enzyme activity can be calculated using the following equation (Cupp-Enyard, 2008):

$$U = \frac{T.V_a}{t.V_c} \tag{10}$$

where U is the amount of enzyme that catalyzes the conversion of 1 µmol substrate per min; T, µmol tyrosine equivalents released; t, time of assay in min; and V_c, volume used in the colorimetric determination in mL.

To evaluate the quantity of tyrosine liberated (T from Eq. 10) during the assay, the absorbance difference between the test sample and the blank sample was calculated.

When the µmol of tyrosine is divided by time in min, it leads to the measurement of protease activity, which is also called as units.

In order to assess the enzyme activity, firstly, a calibration curve was made, relating the absorbance intensity and quantity of the L-Tyrosine liberated. Figure 21 shows the built calibration curve and from it, it is possible to obtain a linear relation between intensity and quantity of the tyrosine:

$$A = 0.951T + 0.004;\ R^2 = 0.9995 \quad (11)$$

where A is the measured absorbance intensity; T, the quantity (in μmol) of the released tyrosine; and R^2, the coefficient of determination.

Figure 21: Calibration curve for enzyme quantification relating absorbance intensity and L-Tyrosine quantity.

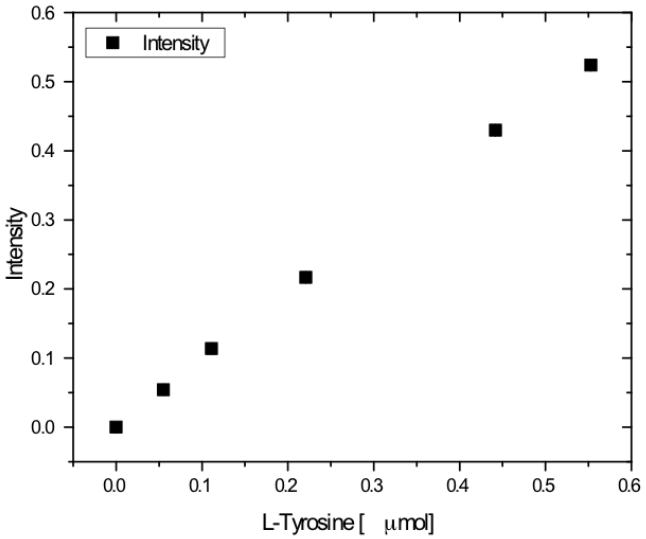

Source: Author.

4 RESULTS AND DISCUSSION

4.1 POWDERS CHARACTERIZATION

Figure 22 shows SEM micrographs of the initial yttria-stabilized zirconia powders. Analyzing the images, it is easily noticeable that the zirconia powders due to the small particle size, thus, high surface area, form conglomerates. Moreover, the particles show a roughly crystalline round shape with a narrow particle size distribution. Comparing the images, it is possible to differentiate two particle sizes.

Figure 22: SEM pictures of the starting powders, TZ-3Y-E (left side) and TZ-3YS-E (right size), 150,000x magnification.

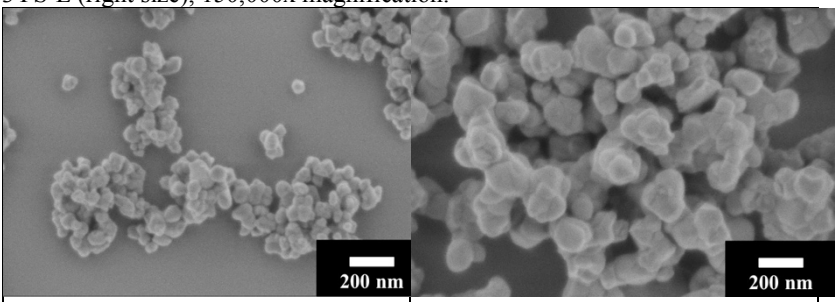

TZ-3Y-E (particle size: 40 nm)	TZ-3YS-E (particle size: 90 nm)

Source: Author.

The average particle size of the powders from the DSL measurements, are shown in Table 2. For TZ-3Y-E and TZ-3YS-E powder, the average particle size was 168 and 238 nm, respectively. These values are higher when compared to the manufacturer's data (40 and 90 nm correspondingly). As seen previously, the zirconia powders form conglomerates, Figure 22. Therefore, it is reasonable to assume that the zirconia conglomerates may be playing an important role in this result. Moreover, two hypotheses can be drawn for the presence of the conglomerates: the ultrasound bath procedure was not totally successful; the agglomerates formed after being broken down and before being analyzed. The second hypothesis is less likely to happen; since a solution with a solution of 1.45 mM of zirconia has a basic character, the particles should be colloidally dispersed and stable, Figure 23.

Table 2: Zirconia manufacturer data and DLS results for average particle size of the zirconia powders.

Material	Manufacturer data (nm)	Measured (nm)
ZYS 40 nm	40	168 ± 9
ZYS 90 nm	90	238 ± 2

Source: Author.

The zeta potential titration of the two powders in suspension shows that the ceramic paste did not require further adjustment in its pH during the processing route. According to Figure 23, in basic media, the suspension showed a stable behavior (Zeta potential > -30 mV, in modulus). Therefore, it is expected that the slurry should remain steady and homogeneous, even during the period of 2 h and thirty min, when it was stored into the extruder's vessel. The isoelectrical point (IEP) for the TZ-3Y-E powder was around the pH 7, while for TZ-3YS-E around 5.

Figure 23: Zeta potential curves of the ceramic precursor powders YSZ 40 nm and 90 nm in a pH range of 2 up to 10 as determined by dynamic laser scattering.

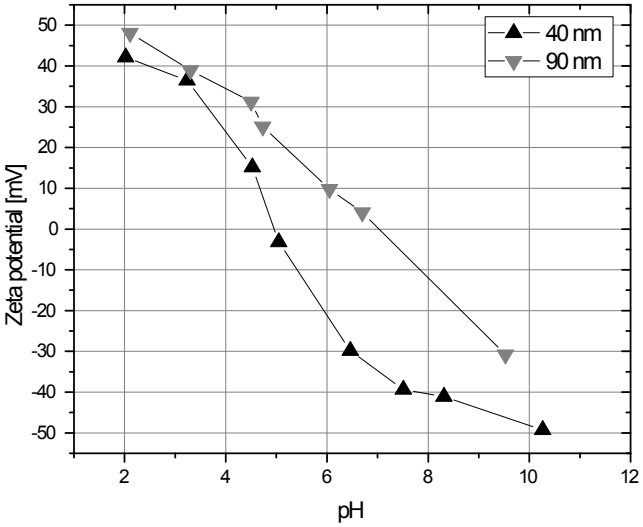

Source: Author.

The specific surface area is calculated from the nitrogen adsorption isotherms, which results are displayed at Table 3. The specific surface area for the zirconia TZ-3Y-E was 13 ± 1 m^2/g while for the TZ-3YS-E 6 ± 1 m^2/g. As stated in the manufacturer's data, the specific surface area should lay around 16 ± 3 and 7 ± 2 m^2/g for TZ-3Y-E and TZ-3YS-E, respectively. Consequently, comparing the measured results with the data offered by the manufacturer, it is possible to observe that they are in accordance.

Table 3: Specific surface area of powders from the manufacturer data and measured BET method.

Material	Manufacturer data (m^2/g)	Measured (m^2/g)
ZYS 40 nm	16 ± 3	12.8 ± 0.5
ZYS 90 nm	7 ± 2	6.0 ± 0.3

Source: Author.

Table 4 displays the result from the helium pycnometry analysis. In the literature, the apparent density value reported for yttria-stabilized zirconia TZ-3Y-E and TZ-3YS-E is around 5800 kg/m^3 (Werner *et al.*, 2014); therefore, the measured results are in accordance with the results published in the literature.

Table 4: Zirconia powders apparent density results from literature (Werner *et al.*, 2014) and the measured helium pycnometry analysis.

Material	Literature (kg/m^3)	Measured (kg/m^3)
ZYS 40 nm	5800	5798 ± 4
ZYS 90 nm	5800	5887 ± 4

Source: Author.

4.2 STRUCTURAL CHARACTERIZATION

In order to make the results and discussion of this specific section more coherent and organized, it is divided into five distinct topics: scanning electron microscopy; optical microscopy; bulk density and open porosity; mercury intrusion porosimetry; and nitrogen adsorption isotherms and BET model.

4.2.1 Scanning electron microscopy

The SEM images in Figure 24 show a partially densified ceramic body; with beginning necks formation among the stabilized zirconia particles. It is in accordance with what was proposed, since a not so high temperature route was employed during the sintering step. Thus, it led to the production of capillaries with high open porosity and satisfactory mechanical stability as it will be shown later (Werner *et al.*, 2014). It is possible to observe that the powder mixture, led to a denser structure. The zirconia powder with the biggest particle size (TZ-3YS-E) caused bigger pore sizes and higher open porosity when compared to the other samples. Moreover, in all conditions. it is noticeable bigger pores in the microstructure, and probably they are a result of the burn out of the sacrificial template (beeswax).

Figure 24: Samples microstructures for different zirconia powders, 50,000x magnification.

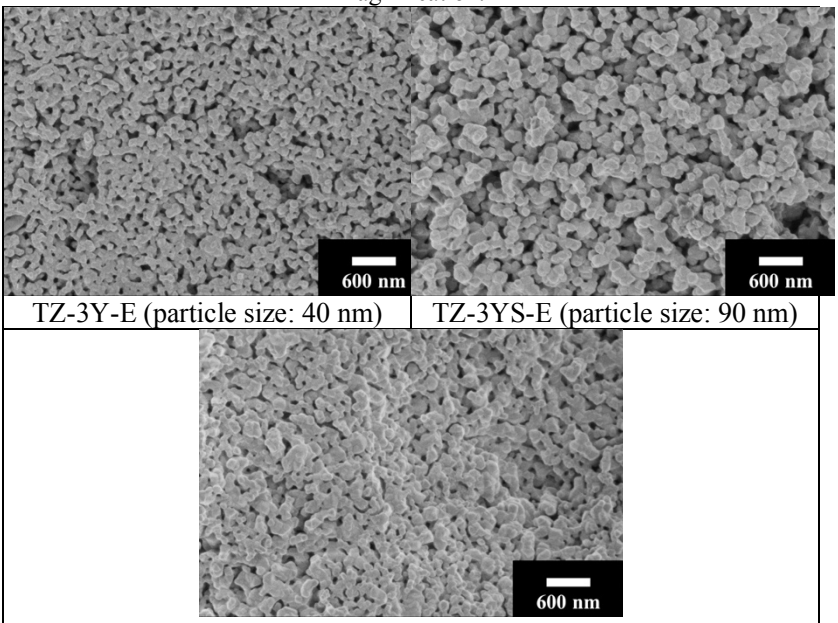

TZ-3Y-E (particle size: 40 nm) | TZ-3YS-E (particle size: 90 nm)

Mixture (particle size: 40/90 nm)

Source: Author.

4.2.2 Optical microscopy

Figure 25 depicts the cross-section images of the porous ceramic microtubes before (left side) and after (left side) sintering. From the pictures, it is not possible to notice any significant difference among the samples. Nevertheless, through the SEM images, the differences are evident.

Figure 25: Optical microscopic images of green (left side) and sintered (right side) capillaries.

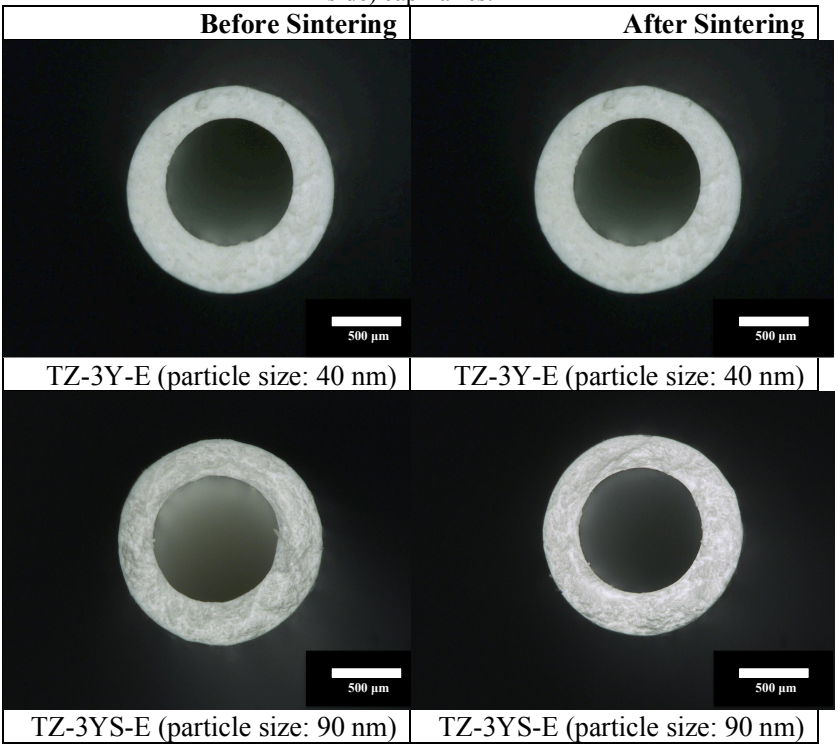

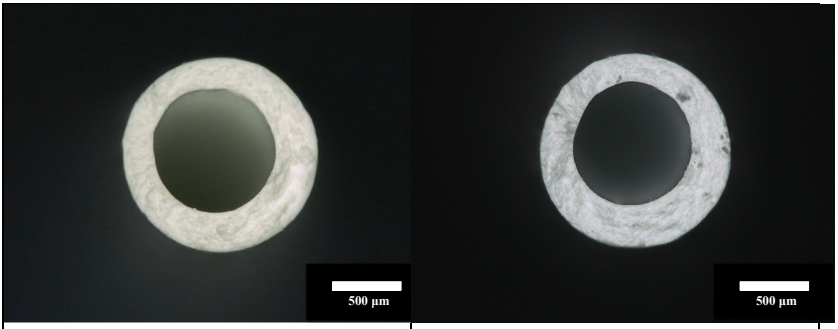

Mixture (particle size: 40/90 nm)	Mixture (particle size: 40/90 nm)

Source: Author.

With the optical images and using the software of the optical microscope it was possible to measure the inner and outer diameter of the capillaries before and after sintering. Table 5 shows the results of the shrinkage of the samples before and after sintering them. These results corroborate with the SEM images, since the blend of powders, was the condition with the highest shrinkage percentage (≈ 12%), while the largest zirconia particle size presented the least shrinkage percentage (≈ 8%). Thus, confirming what was stated before, regarding the visual density of the materials.

Table 5: Shrinkage percentage of capillaries.

Material	Shrinkage outer diameter (%)	Shrinkage inner diameter (%)
ZYS 40 nm	9.51 ± 0.17	10.48 ± 0.17
ZYS 90 nm	7.76 ± 0.15	8.08 ± 0.12
ZYS 40/90 nm	12.75 ± 0.21	11.87 ± 0.22

Source: Author.

4.2.3 Bulk density and open porosity

With reference to the bulk density determined by the geometry and weight of the specimen, again one trend could be observed. Increasing the precursor zirconia particle size led to a decrease in the bulk density, Table 6. As stated previously, the smaller the particle size, the larger is the specific surface area. Additionally, during the sintering stage, using the same sintering conditions, a higher specific surface area is beneficial for the densification of the material.

The results show, again, that the blend of powder presented the highest bulk density (denser material), this could be explained by a better packing of the particles (interstitial packing) during the ceramic processing step (Reed, 1995).

Table 6: Bulk density based on the geometry and mass of the specimens.

Material	Bulk density (kg/m^3)	Std. Dev. (kg/m^3)
ZYS 40 nm	2679	96
ZYS 90 nm	2598	65
ZYS 40/90 nm	2933	93

Source: Author.

Table 7 depicts the calculated theoretical as well as the measure open porosity of the extruded porous microtubes, using Eq.3 and Eq.4. Conforming to the results, capillaries with 53.79 (TZ-3Y-E), 55.86 (TZ-3YS-E), and 49.78 % (Mixture) of open porosity were fabricated.

Table 7: Theoretical and measured open porosity of the samples.

Material	Theoretical porosity (%)	Porosity (%)
ZYS 40 nm	62.86	53.79 ± 0.12
ZYS 90 nm	63.20	55.86 ± 0.09
ZYS 40/90 nm	63.02	49.79 ± 0.14

Source: Author

As can be seen, there is a significant difference (≈ 18%) between the theoretical and measured results. This divergence could be explained by the fact that when the theoretical open porosity was estimated using Eq. 4, the shrinkage of the diameter during the sintering process was neglected, as well as by minor deviations of the diameter along the sample after sintering, and the fact that some decane could volatilize throughout the process.

4.2.4 Mercury intrusion porosimetry

The porous properties of the different capillary types were also investigated using mercury intrusion porosimetry. Figure 26, Figure 27, and Figure 28 show some pieces of information regarding the pore size distributions and the cumulated open porosity of the extruded porous ceramic capillaries. With reference to the open porosity data, they will be neglected in the present work, since the values obtained by the geometry

and weight of the specimens are more reliable. Thus, the focus of this characterization technique will be on the pore size distribution, which is defined by the powder characteristic, composition and processing method (Ojuva *et al.*, 2013).

Figure 26: Intrusion porosimetry in capillaries made of zirconia powder TZ-3Y-E.

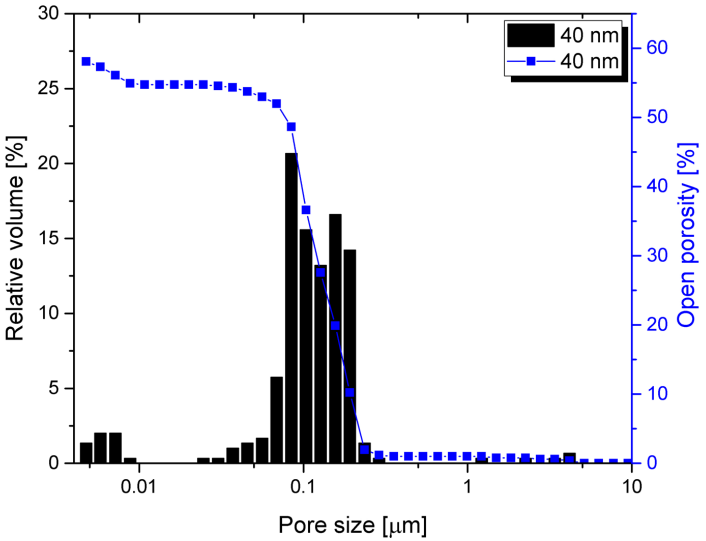

Source: Author.

Figure 27: Intrusion porosimetry in microbes made of zirconia powder TZ-3YS-E.

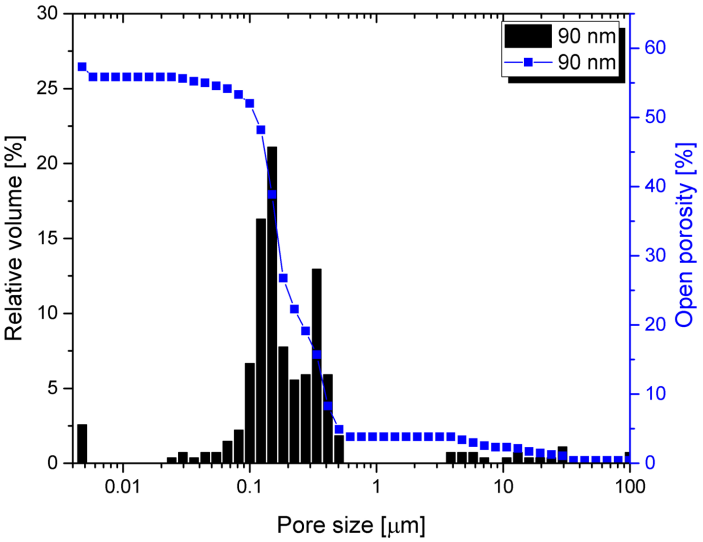

Source: Author.

Figure 28: Intrusion porosimetry in diaphragms made of the mixture of the zirconia powders.

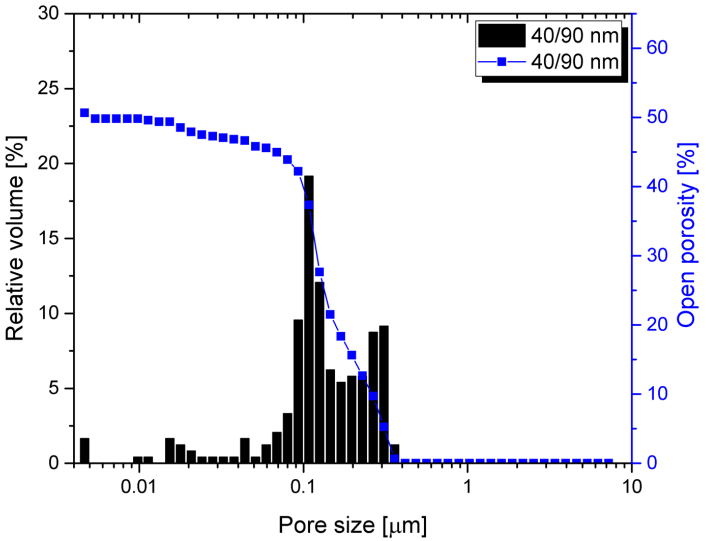

Source: Author.

As stated previously, using the intrusion porosimetry characterization technique, it is possible to detect pores ranging from about 2 nm up to 500 μm (Giesche, 2006). However, this technique is not suitable for very small pore sizes. Analyzing Figure 26, Figure 27, and Figure 28, one can observe the presence of 2 or 3 peaks in relation to the pore size distribution. The first peak lays around 10 nm (0.01 μm) and, probably, it is akin to the inter zirconia particle space. The second peak and the third peak, assign near to 100 nm and 300 nm (0.1 μm and 0.3 μm, respectively) which, possibly, are related to the burnout of the sacrificial template and the aggregates. Moreover, Table 8, suggests that the zirconia with the largest particle size, displayed the highest average pore size and the widest pore size range. On the opposite side, the narrowest pore size range and lowest average pore size was achieved for the smallest zirconia particle size. The mixture of zirconia powders, roughly, displayed an intermediate behavior between the two compositions. Once again, these results are in accordance with the previous one, which is linked with

particles packing and further density after processing and sintering the material.

Table 8: Pore size range and average pore size of the samples.

Material	Pore size range (nm)	Avg. Pore size (nm)
ZYS 40 nm	30 – 250	84
ZYS 90 nm	60 – 500	140
ZYS 40/90 nm	15 – 350	108

Source: Author.

4.2.5 Nitrogen adsorption isotherms and BET model

The specific surface area is calculated from the nitrogen adsorption isotherms. The results are shown in Table 9. A considerable decrease in the specific surface area can be noticed, especially for the TZ-3Y-E capillary, when compared to the powder. This decline originates from the sintering step, due to the formation of necks among the particles, reducing the specific surface area. Additionally, within the sintered extruded ceramic microtubes, it is possible to note that the specific surface area does not vary changing the precursor particle size. The value of the specific surface area lies around 4 m^2/g.

Table 9: Specific surface areas of the sintered capillaries calculated from the nitrogen adsorption isotherms.

Material	Spec. Surf. Area (m^2/g)	Std. Dev. (m^2/g)
ZYS 40 nm	4.21	0.02
ZYS 90 nm	3.97	0.18
ZYS 40/90 nm	4.53	0.05

Source: Author.

4.3 3-POINT BENDING TEST (3PB) AND WEIBULL DISTRIBUTION

For each sample, the maximum bending strength was determined taking into account the highest value in the force-deformation curve and use Eq. 8. Figure 29 shows the Weibull distribution of the flexural strength of the samples, while Table 10 displays the characteristic bending strength and Weibull modulus for each formulation type.

Figure 29: Weibull distribution of 3-point bending test of the sintered zirconia porous capillaries.

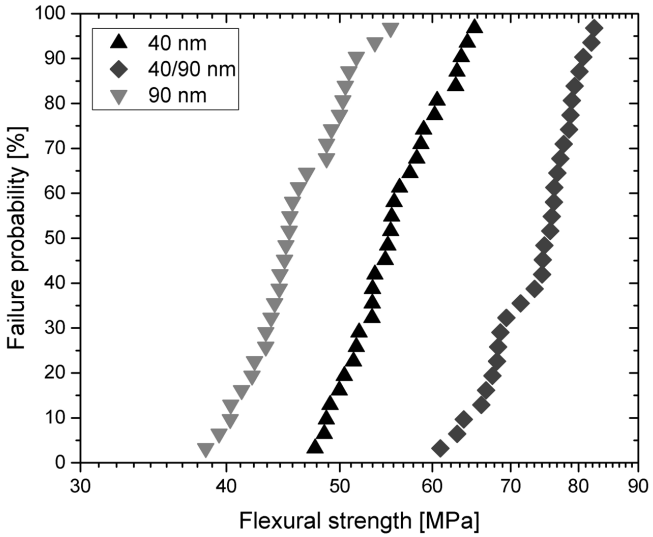

Source: Author.

With reference to the maximum characteristic flexural strength, Table 10, it is possible to verify a trend: increasing the zirconia particle size deteriorated the flexural strength of the capillary. In this case, the open porosity percentage and density play an important role in the mechanical strength (Schaffler e Burr, 1988). The samples with the strongest mechanical stability were the ones made of the blend of the powders, possibly, for being the densest composition with the least open porosity percentage. However, for certain applications, a bending strength of 10 MPa is already suitable for sample handling and utilization (Kroll *et al.*, 2010; Werner *et al.*, 2014).

Table 10: Characteristic flexural strength and Weibull modulus of the ceramic microtubes.

Material	σ_{3PB} (MPa)	Weibull modulus
ZYS 40 nm	57.93	11.77
ZYS 90 nm	47.78	11.27
ZYS 40/90 nm	76.21	15.52

Source: Author.

4.4 WATER PERMEATE FLUX TEST

Figure 30 displays the water permeate fluxes for all the formulation types. Rising the applied pressured led to a linear increase in the water permeate flux. Capillaries made of zirconia TZ-3YS-E, revealed to present the largest water permeate flux.

In the case of the zirconia mixture powders samples, although they had a considerable densification and the lowest open porosity, still they showed, for higher pressures, than TZ-3Y-E. It could be explained by intrinsic permeability of the material.

Figure 30: Water permeate flux tests at different pressures.

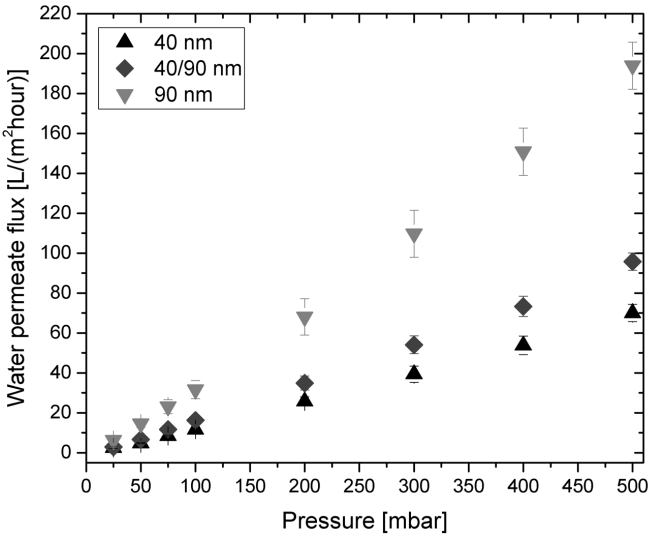

Source: Author.

Permeability is normally assumed as a macroscopic measure that describes the ability to allow the fluid to flow through the voids of a porous medium when compelled by a pressure gradient. Moreover, permeability is not solely a property of the porous medium or the fluid; in contrast, it is a characteristic that reflects the interaction between them. Usually, in laminar flow the permeability is expressed through parameters taken from Darcy's law (Scheffler e Colombo, 2005).

$$-\frac{\Delta P}{L} = \frac{\mu}{k_1} v_s \tag{12}$$

where ΔP is the pressure drop; L is the medium thickness along the flow direction; μ is the absolute viscosity of the fluid; k_1 is the Darcian or intrinsic permeability; and v_s is the superficial fluid velocity.

In this case the fluid velocity can be described as $v_s = Q/A$, where Q is the volumetric flow rate and A is the exposed surface area of the porous medium perpendicular to flow direction (Scheffler e Colombo, 2005; Wikipedia, 2018).

Using the Darcy's law, these are the intrinsic permeability found in the porous tubes: 1.5×10^{-14}, $3.5\text{x}10^{-14}$, and 2.5×10^{-14} m^{-2}, for the TZ-3Y-E, TZ-3YS-E, and blend of powders, respectively. Thus, the intrinsic permeability values explain the water flux results for every condition.

4.5 QUANTIFICATION OF AMINO GROUPS

Figure 31 depicts the quantification of orange dye depending on the silane functionalization route employed. The quantification of orange dye groups was determined using Eq.9. The white bars regard to samples without APTES functionalization, while red bars to samples functionalized in toluene, blue in water, and green in water/ethanol. The solid bars represent samples without hydrothermal activation while the hatched, the ones hydroxylated via autoclave prior to the silanization.

Figure 31: Quantification of orange salt II dye for APTES organic solvent deposition (red bars), aqueous deposition (blue bars), and aqueous/organic solvent deposition (green bars).

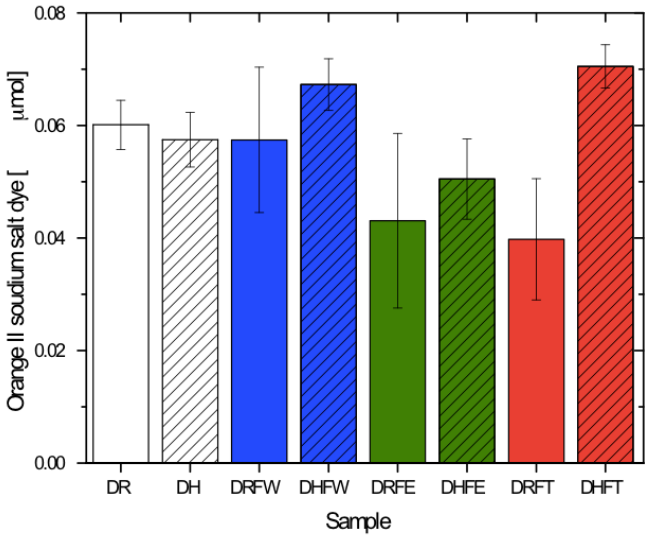

Source: Author.

As can be noted from Figure 31, the samples with more quantity of orange salt II dye; thus, with more amino groups, there are capillaries hydrothermally activated via autoclave and functionalized in toluene (0.070 µmol) and in water (0.067 µmol). Moreover, it is possible to notice that the hydrothermal activation had a favorable influence on the APTES deposition for all the conditions. The hydrothermal step here was important to increase the concentration of OH groups available on the ceramic surface and further silane coupling as shown in Figure 13 and Figure 14.

Even though the samples functionalized via organic solvent (toluene) deposition displayed a slightly better result than the aqueous deposition, the silane deposition in aqueous media was chosen as the functionalization route used in this work. In addition, it was picked as the chosen one, since it is a more environmentally friendly route, it is not so time consuming, and it is a more straightforward method.

Figure 32 shows the result of the amount of amine accessible group attached to the different capillaries types (ZYS 40 nm, hatched dark gray

bar; ZYS 90 nm, hatched light gray bar; and blend of zirconia powder ZYS 40/90 nm, hatched gray bar). As it can be observed, using this approach it was not possible to notice any significant difference among the different types of capillaries. One hypothesis can be drawn, since the specific surface area of all the compositions did not deviate greatly, shown in Table 9, the surface of the capillary was evenly modified among the capillary types. Moreover, the average amine accessible group was approximately 0.170 NH_2 available/nm^2. This result is close to a published work from Kroll et al. (2012), where amine loading capacities between 0.07 and 0.014 NH_2 available/nm^2 were achieved.

Figure 32: Quantification of amine accessible groups for the different types of hydroxylated APTES aqueous functionalized capillaries.

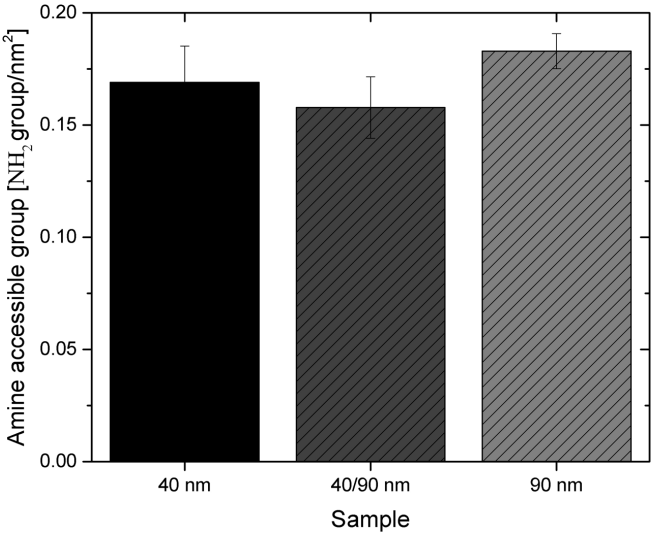

Source: Author.

4.6 ENZYME ACTIVITY UNDER BATCH AND FLOW CONDITIONS

Once calculated the quantity of tyrosine equivalents released, and applying Eq. 9, it is possible to determine the activity of the protease under the batch regime. For this case, it was considered that the volume of essay (V_a) was 10 mL; time of assay (t) was 10 min; and volume used

in colorimetric determination (V_c) was 200 µL. Therefore, basically, the activity of the enzyme is the quantity of tyrosine equivalents liberated multiplied by a factor of five.

The enzyme activity under flow condition was not estimated since the enzyme was not immersed in a casein solution, as it occurred under batch regime. Thus, the volume of assay and time in which the enzyme were in contact with casein are unknown. In pursuance of making the results more comparable, they will be shown in quantity of tyrosine released instead of enzyme activity.

Figure 33 shows the quantification of liberated tyrosine under batch conditions for samples with just hydroxylated surfaces (40H, 40/90H, and 90H) and clicked capillaries (40C, 40/90C, and 90C). All conditions presented a descending behavior up to the third wash, reaching a plateau. The clicked ceramic microtubes exhibited a more moderate drop throughout the washing steps when compared to just hydroxylated condition. One hypothesis could arise from this trend: although the enzyme activity was lower, the enzymes were more strongly attached to the surface due to the click chemistry covalent bonds, indicating a possible success of all the functionalization steps and click chemistry.

In addition, as can be noted, for the first three wash steps, the samples with just hydroxylated treatment, released more tyrosine than the specimens with the whole functionalization process. However, it was expected that clicked capillaries would present the higher amount of liberated tyrosine. This lower amount of tyrosine liberated for the clicked microtubes could be due to the lower initial quantity of enzyme on the support or to a decrease of activity due to steric hindrance and/or blockage of the activity site of the enzyme during the enzyme immobilization step (Hanefeld *et al.*, 2009).

Now, focusing on the hydrothermal activated samples, the tubes made of the biggest zirconia particle size ZYS 90 nm, showed a better performance until being washed up to three times. This could be explained by that the fact of the capillaries exhibiting larger pores and higher porosity was begin for the enzyme activity, avoiding drawbacks such as steric hindrances (Hanefeld *et al.*, 2009).

Figure 33: Quantification of tyrosine equivalents released under batch condition from 1 wash up to 6 washes. M stands for the capillaries made with the mixture (40/90) of zirconia powders.

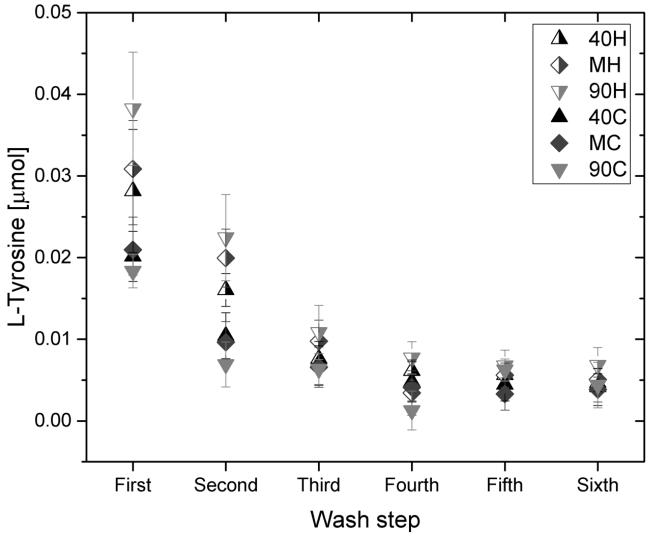

Source: Author.

Figure 34 displays the quantification of released tyrosine under flow regime after 10, 20, and 30 min of test, for samples with just hydroxylated surfaces (40H, 40/90H, and 90H) and clicked capillaries (40C, 40/90C, and 90C). In this test, almost all samples did not show any significant release of tyrosine, except for the clicked capillary made of zirconia with the largest particle size (ZYS 90 nm). Therefore, some hypothesis could be drawn. First, for this type of regime, the assay was just started when a flow rate of 0.2 mL/min was settled. So, prior to collecting the material, the during the adjustment of the flow rate, the enzymes were leached out by reason of high pressures within the capillaries. Second, the clicked ZYS 90 nm microtubes could exhibit any performance, as a result of the larger pores and open porosity aligned with the covalent bonds prevenient from the click chemistry.

As shown in the water permeate test results, Figure 30, fixing a certain water flux, the microtubes made of ZYS 90 nm displayed lower pressures; thus, for flow condition, it is expected that less enzyme is leached out. One can observe that in both, batch and flow regimes, the

higher amount of tyrosine liberated was found for specimens made with the biggest zirconia particle size (ZYS 90 nm). This better performance, when compared to the other conditions, could be associated with a larger space for enzyme activity, avoiding enzyme steric hindrance, and in the case of flow regime, lower pressures used in the process, preventing leaching out the enzymes (Hanefeld *et al.*, 2009). The clicked samples showed promising results for both test conditions.

Figure 34: Quantification of L-Tyrosine equivalents liberated under flow condition, after 10, 20, and 30 min of test. M stands for the capillaries made with the mixture (40/90) of zirconia powders.

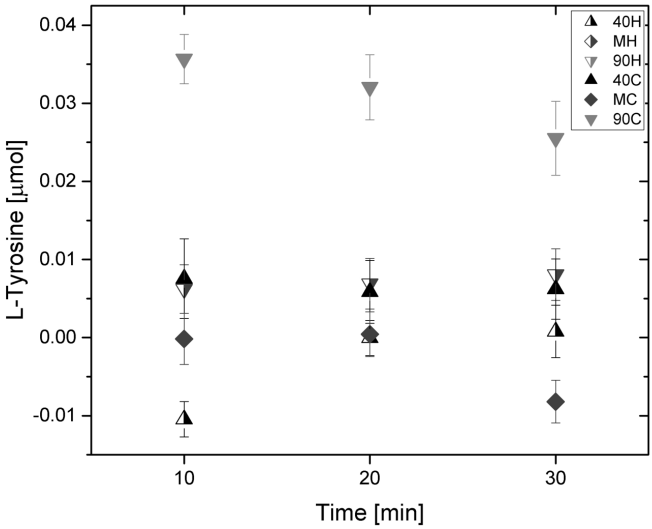

Source: Author.

5 CONCLUSIONS

Yttria-stabilized porous zirconia microtubes were successfully produced combining the extrusion molding process and the sacrificial template technique. As starting materials, two different zirconia particle size powders, decane, hexane, stearic acid, and beeswax were chosen. The zirconia powders had a roughly spherical shape, and due to their small size, they tended to form agglomerates. The zirconia isoelectric point was found to be at pH of 7 for TZ-3Y-E (ZYS 40 nm) and at pH 5 for TZ-3YS-E (ZYS 90 nm). The prepared ceramic paste seemed to be colloidally stable in basic media. The measured specific surface area and the apparent density of the zirconia powders are in accordance with the results published in the literature and by the supplier.

Relating to compressive strength, a pattern was reached: decreasing the zirconia particle size increased the characteristic flexural strength of the microtubes. However, the strongest samples were made by combining both powders. Moreover, the mixture of zirconia powders also led to capillaries displaying the highest bulk density. This result is in consonance with the SEM and OM pictures as well as the 3-point bending test. Therefore, one can conclude that using different starting particle size can be beneficial for a better packing of the material, encompassing higher densities.

In terms of water permeate flux, it showed an antagonistic trend when compared to the compressive strength. As the zeolite particle size rose, the greater was the water permeate flux. This could be explained by the intrinsic permeability, where it showed an opposite behavior when compared to the water permeate flux tendency.

Regarding to open porosity and pore size range, microtubes displaying open porosity from 50% to 56 % were fabricated. The samples made with the bigger zirconia particle size gave rise to the highest open porosity as well as the widest pore size range. These divergences in open porosity percentage and pore size range played a role on the intrinsic permeability values.

With respect to the surface functionalization, it was observed that a hydroxylation step prior to APTES deposition was benign. Furthermore, an average amine accessible group of 0.170 NH_2 available/nm^2 was reached and it seemed that the composition of the capillaries did not present a significant effect on the APTES deposition. Nevertheless, for the enzyme activity, it was observed that the specimens made of the largest zirconia particle size, led to better enzyme activity results. For the enzyme activity tests under batch condition, it was not possible to notice

a direct improvement of the enzyme activity using click chemistry as an immobilization technique. However, it seemed that the click chemistry functionalized samples displayed a more stable behavior throughout the washes steps. Moving to the enzyme activity tests under flow regime, the results suggested that the enzymes were leached out even before starting the measurement of the test for almost all conditions, except for the clicked microtube made of the biggest zirconia particle size (ZYS 90 nm). Therefore, for the aim of this work, the optimum sample was made with zirconia TZ-3YS-E (ZYS 90 nm) with click chemistry.

As prospective works would be interesting to produce capillaries with different sacrificial templates in order to play with the open porosity and average pore size and asses their influence on the enzyme activity. It is advisable to use other means of characterization techniques for the functionalized microtubes such as SIRS, FTIR, TGA, and zeta potential to evaluate the success of each functionalization step. Finally, it is suggested to conduct enzyme activity experiments, using different parameter (flow rate, casein concentration, and time of tests).

REFERENCES

AI, Q. et al. Highly efficient covalent immobilization of catalase on titanate nanotubes. **Biochemical Engineering Journal,** v. 83, p. 8-15, 2014/02/15/ 2014. ISSN 1369-703X. Disponível em: < http://www.sciencedirect.com/science/article/pii/S1369703X13003379 >.

AKHTAR, F. et al. Structuring adsorbents and catalysts by processing of porous powders. **Journal of the European Ceramic Society,** v. 34, n. 6, p. 1643-1666, 2014.

AL-ZUHAIR, S. et al. Enzymes in Biofuels Production. **Enzyme Research,** v. 2011, n. 2011, p. 1-2, 2011.

ARSHAD, M. S. et al. Plant and bacterial proteases: A key towards improving meat tenderization, a mini review. **Cogent Food & Agriculture,** v. 2, n. 1, p. 1261780, 2016/12/31 2016. ISSN null. Disponível em: < https://www.tandfonline.com/doi/abs/10.1080/23311932.2016.1261780 >.

BAJPAI, P. Application of Enzymes in the Pulp and Paper Industry. **Biotechnology Progress,** v. 15, n. 2, p. 147-157, 1999. Disponível em: < https://onlinelibrary.wiley.com/doi/abs/10.1021/bp990013k >.

BAPTISTA, J. L.; LUCAS, D. B. **Introdução à ciência e tecnologia dos materiais cerâmicos**

BOCH, P.; NIEPCE, J.-C. **Ceramic Materials: Processes, Properties, and Applications**. 2007. 573.

BRUNAUER, S.; EMMETT, P. H.; TELLER, E. Adsorption of Gases in Multimolecular Layers. **Journal of the American Chemical Society,** v. 60, n. 2, p. 309-319, 1939.

CASTRO, V.; RODRÍGUEZ, H.; ALBERICIO, F. CuAAC: An Efficient Click Chemistry Reaction on Solid Phase. **ACS Combinatorial Science,**

v. 18, n. 1, p. 1-14, 2016/01/11 2016. ISSN 2156-8952. Disponível em: < https://doi.org/10.1021/acscombsci.5b00087 >.

COLOMBO, P. Conventional and novel processing methods for cellular ceramics. **Philosophical Transaction of the Royal Society,** v. 2006, n. 364, p. 109-124, 2005.

CUPP-ENYARD, C. Sigma's Non-specific Protease Activity Assay - Casein as a Substrate. **Journal of Visualized Experiments,** v. 899, n. 19, 2008.

DATTA, S.; CHRISTENA, L. R.; RAJARAM, Y. R. S. Enzyme immobilization: an overview on techniques and support materials. **3 Biotech**, Berlin/Heidelberg**,** v. 3, n. 1, p. 1-9, 06/06
02/02/received
05/20/accepted 2013. ISSN 2190-5738. Disponível em: < http://www.ncbi.nlm.nih.gov/pmc/articles/PMC3563746/ >.

DAUGAARD, A. E.; HVILSTED, S. **Functional Materials by Click Chemistry**. Technical University of Denmark 2009.

DEVILLE, S. Freeze-Casting of Porous Ceramics: A Review of Current Achievements and Issues. **Advanced Engineering Materials,** v. 10, n. 3, p. 1527-2648, 2008.

DIETERICH, F. et al. Development and characterization of protein hydrolysates originated from animal agro industrial byproducts. **J Dairy Vet Anim Res,** v. 1, 2014. Disponível em: < https://doi.org/10.15406/jdvar.2014.01.00012 >.

EPA, U. S. The brownfields and land revitalization technology support center. Disponível em: < http://www.brownfieldstsc.org/glossary.cfm?q=1 >. Acesso em: February, 9th.

GIBSON, L. J.; ASHBY, M. F. **Cellular Solids: Structure and Properties**. Franklin book, 1988. Disponível em: < https://books.google.com.br/books?id=IxPFoAEACAAJ >.

GIESCHE, H. Mercury Porosimetry: A General (Practical) Overview. **Particle & Particle Systems Characterization,** v. 23, n. 1, p. 1-11, 2006.

GODFREY, T.; REICHELT, J. **Industrial enzymology: the application of enzymes in industry**. New York, NY, USA: Nature Press, 1982.

GOLE, A.; MURPHY, C. J. Azide-Derivatized Gold Nanorods: Functional Materials for "Click" Chemistry. **Langmuir,** v. 24, n. 1, p. 266-272, 2008.

HANEFELD, U.; GARDOSSI, L.; MAGNER, E. Understanding enzyme immobilisation. **Chemical Society Reviews,** v. 38, n. 2, p. 453-468, 2009. ISSN 0306-0012. Disponível em: < http://dx.doi.org/10.1039/B711564B >.

HERMANSON, G. T. **Bioconjugate Techniques**. Third. Academic Press, 2013.

HOU, Y. et al. Protein hydrolysates in animal nutrition: Industrial production, bioactive peptides, and functional significance. **Journal of Animal Science and Biotechnology,** v. 8, n. 1, p. 24, March 07 2017. ISSN 2049-1891. Disponível em: < https://doi.org/10.1186/s40104-017-0153-9 >.

HÄNDLE, F. **Extrusion in ceramics**. Berlin ; New York: Springer, 2007. ISBN 9783540271000 (hardcover : alk. paper).

ISOBE, T. et al. Preparation and properties of porous alumina ceramics with oriented cylindrical. **Journal of the European Ceramic Society,** v. 26, n. 6, p. 958-960, 2006.

JULBE, A.; FARRUSSENG, D.; GUIZARD, C. Porous ceramic membranes for catalytic reactor - overview and new ideas. **Journal of Membrane Science,** v. 181, n. 1, p. 3-20, 2001.

KAUFMANN, J. Mercury Intrusion Porosimetry. 2017. Disponível em: < http://www.empa.ch/plugin/template/empa/*/95361 >. Acesso em: February, 8th.

KEULEN, J. V. Density of porous solids. **Matériaux et Construction,** v. 6, n. 3, p. 181-183, 1973.

KOLB, H. C.; FINN, M. G.; SHARPLESS, K. B. Click Chemistry: Diverse Chemical Function from a Few Good Reactions. **Angewandte Chemie (International ed. in English),** v. 40, n. 11, p. 2004-2021, 2001.

KOLB, H. C.; SHARPLESS, K. B. The growing impact of click chemistry on drug discovery. **Drug Discovery Today,** v. 8, n. 24, p. 1128-1137, 2003/12/15/ 2003. ISSN 1359-6446. Disponível em: < http://www.sciencedirect.com/science/article/pii/S1359644603029337 >.

KOOPMAN, R. et al. Ingestion of a protein hydrolysate is accompanied by an accelerated in vivo digestion and absorption rate when compared with its intact protein. **The American Journal of Clinical Nutrition,** v. 90, n. 1, p. 106-115, 2009. ISSN 0002-9165. Disponível em: < http://dx.doi.org/10.3945/ajcn.2009.27474 >.

KROLL, S. et al. Highly Efficient Enzyme-Functionalized Porous Zirconia Microtubes for Bacteria Filtration. **Environmental Science & Technology,** v. 46, n. 16, p. 8739-8747, 2012.

_____. Development and characterisation of functionalised ceramic microtubes for bacteria filtration. **Journal of Membrane Science,** v. 365, n. 1, p. 447-455, 2010.

KUMAR, S. Role of enzymes in fruit juice processing and its quality enhancement. **Advances in Applied Science Research,** v. 6, n. 6, p. 114-124, 2015.

LEARNING, C. Adsorption Isotherm. 2009. Disponível em: < http://www.chemistrylearning.com/adsorption-isotherm/ >. Acesso em: February, 9th.

LEE, M.; WU, Z.; LI, K. 2 - Advances in ceramic membranes for water treatment. In: (Ed.). **Advances in Membrane Technologies for Water Treatment**. Oxford: Woodhead Publishing, 2015. p.43-82. ISBN 978-1-78242-121-4.

LEE, W. E.; RAINFORTH, M. **Ceramic Microstructures: Property control by processing**. Springer Netherlands, 1994. 590.

LIANG, L.; ASTRUC, D. The copper(I)-catalyzed alkyne-azide cycloaddition (CuAAC) "click" reaction and its applications. An overview. **Coordination Chemistry Reviews,** v. 255, n. 23, p. 2933-2945, 2011/12/01/ 2011. ISSN 0010-8545. Disponível em: < http://www.sciencedirect.com/science/article/pii/S0010854511001809 >.

LIU, P. S.; CHEN, G. F. **Porous materials processing and applications**. 2014.

MEDICINE, I. O. **Dietary Reference Intakes for Energy, Carbohydrate, Fiber, Fat, Fatty Acids, Cholesterol, Protein and Amino Acids**. Washington, DC, USA: National Academy Press, 2005.

MERRIAM-WEBSTER. Cell. Merriam-Webster, 2018. Disponível em: < http://www.merriam-webster.com/dictionary/cell >. Acesso em: January, 29th.

MOEHLENBROCK, M. J.; MINTEER, S. D. Introduction to the Field of Enzyme Immobilization and Stabilization. In: MINTEER, S. D. (Ed.). **Enzyme Stabilization and Immobilization: Methods and Protocols**. New York, NY: Springer New York, 2017. p.1-7. ISBN 978-1-4939-6499-4.

MOHAMAD, N. R. et al. An overview of technologies for immobilization of enzymes and surface analysis techniques for immobilized enzymes. **Biotechnology, Biotechnological Equipment,** v. 29, n. 2, p. 205-220, 02/17
08/27/received
10/07/accepted 2015. ISSN 1310-2818
1314-3530. Disponível em: < http://www.ncbi.nlm.nih.gov/pmc/articles/PMC4434042/ >.

MOSES, J. E.; MOORHOUSE, A. D. The growing applications of click chemistry. **Chemical Society Reviews,** v. 36, n. 8, p. 1249-1262, 2007. ISSN 0306-0012. Disponível em: < http://dx.doi.org/10.1039/B613014N >.

NORMUNG, D. I. F. **Advanced technical ceramics - Mechanical properties of monolithic ceramics at room temperature - Part 1: Determination of flexural strength** 2008.

OJUVA, A. et al. Laminated Adsorbents with Very Rapid CO2 Uptake by Freeze-Casting of Zeolites. **CS Applied Materials & Interfaces,** v. 5, n. 7, p. 2669-2676, 2013.

PANALYTICAL, M. Zeta potential. Disponível em: < http://www.malvern.com/labeng/technology/zeta_potential/zeta_potential_lde.htm >. Acesso em: February, 8th.

PASUPULETI, V. K.; BRAUN, S. State of the Art Manufacturing of Protein Hydrolysates. In: PASUPULETI, V. K. e DEMAIN, A. L. (Ed.). **Protein Hydrolysates in Biotechnology**. Dordrecht: Springer Netherlands, 2010. p.11-32. ISBN 978-1-4020-6674-0.

PAULOVÁ, L.; PATÁKOVÁ, P.; BRÁNYIK, T. **Advanced Fermentation Processes**. 2013. 89-105 ISBN 9781439895450.

PLUEDDEMANN, E. P. **Silane coupling agents**. New York ; London: Plenum, 1982. ISBN 0306409577 : Unpriced.

PUJALA, R. K. **Dispersion stability, microstructure and phase transition of anisotropic nanodiscs**. Springer, 2014.

QUINN, G. et al. Flexural Strength of Ceramic and Glass Rods. 2009.

REED, J. S. **Principles of ceramic processing**. Second. New York: Wiley-Interscience, 1995.

ROUQUEROL , J. et al. *Recommendations for the characterization of porous solid (Technical Report)*. **Pure and Applied Chemistry,** v. 66, n. 8, p. 1739-1758, 1994.

SCHAFFLER, M. B.; BURR, D. B. Stiffness of compact bone: Effects of porosity and density. **Journal of Biomechanics,** v. 21, n. 1, p. 13-16, 1988/01/01/ 1988. ISSN 0021-9290. Disponível em: < http://www.sciencedirect.com/science/article/pii/0021929088901868 >.

SCHEFFLER, M.; COLOMBO, P. **Cellular ceramics : structure, manufacturing, properties and applications**. Weinheim: Wiley-VCH ; Chichester : John Wiley [distributor], 2005. ISBN 9783527313204 (hbk.) : ¹175.00
3527313206 (hbk.) : ¹175.00.

SEEBER, B. S. M.; GONZENBACH, U. T.; GAUCKLER, L. J. Mechanical properties of highly porous alumina foams. **Journal of materials research,** v. 28, n. 17, p. 2281-2287, 2013.

SEWCZYK, T. et al. Flow rate dependent continuous hydrolysis of protein isolates. **AMB Express**, Berlin/Heidelberg**,** v. 8, p. 18, 02/10 11/14/received
02/05/accepted 2018. ISSN 2191-0855. Disponível em: < http://www.ncbi.nlm.nih.gov/pmc/articles/PMC5812119/ >.

SING, K. S. W. et al. Reporting Physisorption data for
gas/solid systems with Special Reference to the Determination of Surface Area
and Porosity. **Pure and Applied Chemistry,** v. 57, n. 4, p. 603-619, 1985.

SOUSA JR, R. et al. Kinetic model for whey protein hydrolysis by alcalase multipoint-immobilized on agarose gel particles. **Brazilian Journal of Chemical Engineering,** v. 21, p. 147-153, 2004. ISSN 0104-6632. Disponível em: < http://www.scielo.br/scielo.php?script=sci_arttext&pid=S0104-66322004000200003&nrm=iso >.

STUDART, A. R. et al. Processing Routes to Macroporous Ceramics: A Review. **Journal of the American Ceramic Society,** v. 89, n. 6, p. 1771–1789, 2006.

TRECCANI, L. et al. Functionalized ceramics for biomedical, biotechnological and environmental applications. **Acta Biomaterialia,** v. 9, n. 7, p. 7115-7150, 2013.

TURNBOUGH, M.; MARTOS, M. What are proteins. 2003. Disponível em: < https://askabiologist.asu.edu/venom/what-are-proteins >. Acesso em: March, 13.

UNIVERSITY, U. **Derivation of BET and Langmuir Isotherms** 2011.

WEBB, P. A. O., CLYDE. **Analytical methods in fine particle technology**. Micromeritics Instrument, 1997.

WEIBULL, W. A statistical distribution function of wide applicability. **Journal of Applied Mechanics,** v. 18, p. 293-297, // 1951.

WERNER, J. et al. Production of ceramic membranes with different pore sizes for virus retention. **Journal of Water Process Engineering,** v. 4, p. 201-211, 2014.

WIKIPEDIA. Método de BET. 2017. Disponível em: < http://pt.wikipedia.org/wiki/M%C3%A9todo_de_BET >.

_____. Darcy's law., 2018. Disponível em: < http://en.wikipedia.org/wiki/Darcy%27s_law >. Acesso em: February, 18th.

ZHENG, M. et al. A mixed-function-grafted magnetic mesoporous hollow silica microsphere immobilized lipase strategy for ultrafast transesterification in a solvent-free system. **RSC Advances,** v. 5, n. 54, p. 43074-43080, 2015. Disponível em: < http://dx.doi.org/10.1039/C5RA05611J >.

ZILLI, M. **Internship Report**. Advanced Ceramics. Bremen. 2016

ZIMMERMAN, M.; SNOW, B. **An Introduction to Nutrition**. Creative Commons, 2012.